ACADEMIC PRESS

Available online at www.sciencedirect.com

SCIENCE DIRECT®

Journal of Computational Physics 184 (2003) 79–105

JOURNAL OF COMPUTATIONAL PHYSICS

www.elsevier.com/locate/jcp

High-resolution viscous flow simulations at arbitrary Mach number

W.R. Briley[a,*,1], L.K. Taylor[a,b,1], D.L. Whitfield[b,1]

[a] *Mechanical Engineering, Computational Simulation and Design Center, Mississippi State University, Mississippi State, MS 39762, USA*

[b] *Aerospace Engineering, Computational Simulation and Design Center, Mississippi State University, Mississippi State, MS 39762, USA*

Received 13 July 2001; received in revised form 4 September 2002; accepted 29 September 2002

Abstract

A characteristic-based unsteady viscous flow solver is developed with preconditioning that is uniformly applicable for Mach numbers ranging from essentially incompressible to supersonic. A preconditioned flux-difference formulation for nondimensional primitive variables is a key element of the present approach. The simple primitive-variable numerical flux is related to Roe's flux-difference scheme and preserves contact discontinuities using primitive variables, with or without preconditioning. Preconditioning by a single-parameter diagonal matrix conditions the system eigenvalues in terms of nondimensional local velocity and local temperature. An iterative implicit solution algorithm is given for the preconditioned formulation and is used for several simple test and validation cases. These include an inviscid shock-tube case, flat-plate boundary layer flow at low Mach number, viscous flow past a circular cylinder at low Reynolds number and with different thermal boundary conditions, and validation cases for incompressible and transonic flows.

Keywords: Preconditioning; Flux-difference; Implicit; Unsteady; Viscous; Approximate factorization; Discontinuity; Characteristic; Simulation

1. Introduction

Numerical algorithms for viscous compressible flow face well-known difficulties for low Mach number conditions. If the total enthalpy is constant (isoenergetic flow), then steady solutions approach the incompressible constant-density limit as Mach number approaches zero. Such problems are often solved using the incompressible flow equations and artificial compressibility formulations. Low-speed flows with

* Corresponding author. Tel.: 1-423-648-3166; fax: 1-423-648-3169.

E-mail addresses: roger-briley@utc.edu (W.R. Briley), lafe-taylor@utc.edu (L.K. Taylor), dave-whitfield@utc.edu (D.L. Whitfield).

[1] Present address: Graduate College of Computational Engineering, University of Tennessee at Chattanooga, Grote 223, 615 McCallie Avenue, Chattanooga TN 37403, USA.

0021-9991/02/$ - see front matter
PII: S0021-9991(02)00018-9

heat transfer have variable density, and thus incompressible formulations are not suitable. It has long been observed that the stability and/or convergence properties of most compressible flow algorithms is degraded for low Mach number flows. A number of preconditioning techniques have been developed to overcome these difficulties, and recent review articles by Turkel [1,2] give detailed accounts of many of these techniques. A discussion of previous related work on preconditioning methods for arbitrary Mach number and related characteristic-based flux approximations for viscous flow applications will help to provide context for the present formulation. Some discussion of iterative implicit unsteady flow solvers is also given.

1.1. Preconditioning for arbitrary Mach number

A simple preconditioning technique was introduced by Briley et al. [3] to improve the convergence rate of an implicit ADI approximate-factorization scheme applied to the steady isoenergetic Navier–Stokes equations at low Mach number. Introducing nondimensional variables with reference Mach number M_r, a constant preconditioning matrix $\mathrm{diag}(1/\gamma M_r^2, 1, 1)$ was added to the isoenergetic equations to remove an ill-conditioned behavior in the approximate-factorization error at low Mach number. This technique greatly improved the convergence rate at $M_r = 0.05$ for turbulent flow through a 90° channel bend. The isoenergetic formulation is applicable to steady isoenergetic viscous or inviscid flow at arbitrary Mach number and had been used earlier by McDonald and Briley [4] for supersonic flows. Steger and Kutler [5] identified factorization error as a source of difficulty at low Mach number.

Choi and Merkle [6] studied the convergence of implicit solutions for both one and two-dimensional inviscid test problems. Their results gave further detailed evidence that poor convergence at low Mach number is associated with factorization errors in the implicit algorithm, and only indirectly with stiffness in the system eigenvalues. They then addressed this problem by introducing a preconditioning matrix $\mathrm{diag}(1, 1, 1, M^{-2})$ into the compressible Euler equations written in (ρ, u, v, p) variables. These equations were then transformed to conservative variables $(\rho, \rho u, \rho v, e_t)$ for solution. At $M = 0.05$, this method gave convergence rates identical to those using the artificial compressibility equations. This preconditioning is similar to that of [3] but distinct since it is not restricted to isoenergetic flows, and it is implemented using conservative variables. Merkle and Choi [7] later concluded that the scheme of [6] was not adequate for inviscid flow below $M = 0.01$ and developed a perturbation expansion approximation that gave convergence rates independent of Mach number as low as 10^{-5}, for a duct flow with substantial heat addition.

Viviand [8] gave a systematic study of pseudo-unsteady first-order systems for steady inviscid flow calculations. A general parametric family of first-order systems for steady compressible isoenergetic flow calculations was defined, subject to conditions of hyperbolicity and a condition on the number of negative eigenvalues.

Turkel [9] devised a generalized preconditioning matrix for the artificial compressibility method in (p, u, v) variables that includes time derivative terms analogous to those in [3]. He also applied this generalization to the compressible equations in terms of (p, u, v, S), (p, u, v, ρ), and isoenergetic variables (p, u, v), thus providing unification of several existing compressible and artificial compressibility approaches. Turkel suggested a preconditioning parameter based on the local velocity, with a limiter to avoid singular behavior near stagnation points. Briley et al. [10] compared Turkel's artificial compressibility formulation [9] with the preconditioned isoenergetic compressible formulation of [3], using the same implicit algorithm. Both of these formulations gave essentially the same convergence behavior for a viscous flow at Mach numbers between 10^{-3} and 0.5, without using a local preconditioning parameter.

Choi and Merkle [11] concluded that the preconditioning of [6] was not effective for viscous flows and proposed a new preconditioning for viscous variable Mach number flows, based on (p, u, v, T) variables. These preconditioned equations are similar to the perturbation equations of [7] but include a mechanism for controlling inviscid and viscous time-step parameters. The preconditioning matrix contains separate inviscid (βM^2) and viscous (δ) parameters, where M is a local Mach number modified with a limiter to

avoid singular behavior near stagnation points. This method was found to be effective at low Mach number for several test calculations ranging from inviscid to highly viscous flows.

Weiss and Smith [12,13] developed a preconditioning matrix related to that of [11], using (p, u, v, T) variables and without assuming an ideal gas. It is implemented with a Roe-type flux-difference splitting and an explicit multistage algorithm, with dual time stepping for unsteady flows. Pletcher and Chen [14] developed a preconditioned iterative unsteady formulation, with pseudo-time derivative terms preconditioned by a constant matrix $\mathrm{diag}(1/\gamma M_r^2, 1, 1, 1)$ and using nondimensional (p, u, v, T) variables. Edwards and Liou [15] have developed extensions of the advective upwind splitting method (AUSM) for all flow speeds. They employ the preconditioning matrix $\boldsymbol{\Gamma}$ of Choi and Merkle [11], as extended by Weiss and Smith [12]. This scheme is successfully demonstrated for several two-dimensional viscous and inviscid flows over a wide range of Mach numbers. Edwards and Thomas [16] utilize the Weiss–Smith [12] preconditioning and a Roe-type scheme based on primitive variables (ρ, u, v, p).

In his recent review article, Turkel [2] gives two motivations for preconditioning: (1) preconditioning of time derivatives to accelerate convergence and (2) modification of upwinding schemes or artificial dissipation for central differences to achieve accuracy at low Mach numbers. Accordingly, the preconditioning matrix for time derivatives is treated separately from that included with dissipation terms. The treatment given is very general and includes centered schemes with scalar or matrix dissipation as well as upwind schemes. The closely related preconditionings of Turkel [9], Choi and Merkle [11], and Weiss and Smith [12] are compared, and the selection of preconditioning parameters and local limiters are discussed in detail.

1.2. High-resolution inviscid fluxes for viscous flows

A review article by Roe [17] discusses the emergence of characteristic-based approximations for the compressible Euler equations. A more recent and comprehensive account of methods based on Riemann solvers is given by Toro [18]. These schemes specifically address the presence of shocks and other discontinuities. Perhaps the most widely used is Roe's flux-difference scheme [19], which employs an exact solution to an approximate Riemann problem to define a set of averaged variables and fluxes that preserve one-dimensional discontinuities at cell interfaces. The primitive-variable flux formulation introduced here is derived as a modification of Roe's flux.

For viscous flow, there is evidence that accurate resolution of thin shear layers is enhanced by characteristic-based inviscid approximations that preserve contact or shear discontinuities known as slip lines in compressible flows and as vortex shests in incompressible flows. Roe's flux [19] and the AUSM flux of Liou and Steffan [20] are examples of fluxes that preserve contact discontinuities. Evidence of improved viscous resolution using an implementation of Roe's flux is given by Simpson and Whitfield [21], who demonstrated that the Blasius solution could be resolved with as few as 3–4 grid points defining the boundary layer profile. In the present authors' experience, schemes that do not preserve inviscid discontinuities require higher resolution. The primitive-variable inviscid flux formulation developed here also exactly satisfies slip-line discontinuities, with or without preconditioning, and hence provides high resolution of viscous flows at high Reynolds number.

1.3. Present preconditioned flux-difference formulation

The present study seeks to develop a single high-resolution unsteady viscous flow solver with preconditioning that is uniformly applicable for Mach numbers ranging from essentially incompressible to supersonic. A preconditioned inviscid flux-difference formulation for primitive variables is a key element of the present approach. A simple preconditioned flux related to Roe's flux-difference scheme [19] is developed that preserves contact discontinuities using primitive variables, with or without preconditioning. This property is considered to be advantageous for viscous flows at high Reynolds number. A nondimension-

alization as in [3] extracts the single parameter M_r representing the global scaling of variables in the system of equations and boundary conditions. Preconditioning by diag$[1, 1, 1, \beta(M_r)]$ with the primitive-variable choice $\boldsymbol{q} \equiv (\rho, u, v, w, p)^T$ provides O(1) eigenvalues that depend on local velocity and sound speed and also leads to very simple eigensystems. The system reduces to its unpreconditioned form for $\beta = 1$, giving a particularly simple flux-difference scheme in primitive variables.

The present preconditioning resembles that of [3] in its use of a constant diagonal matrix based on nondimensional primitive variables. The diagonal preconditioning matrix used here has the same form as that of Choi and Merkle [6], except that a constant global parameter $\beta(M_r)$ replaces the local Mach number of [6]. It will later be shown that the resulting preconditioned eigenvalue behavior is fundamentally different near stagnation points and for large temperature variation. The present method has not encountered difficulty in viscous flows, as reported by Choi and Merkle [11], and has not required viscous preconditioning parameters, as used in [11,12,15,16]. The present method also differs from that of [6] and [11] in its use of characteristic-based primitive-variable fluxes and an iterative implicit algorithm. Finally, the Roe-type flux-difference approach used here is similar to that used in [12,16] but the present eigensystems and flux formulas are different due to the preconditioning.

1.4. Iterative implicit algorithm

The present preconditioned primitive-variable formulation is solved using an iterative implicit discretized-Newton scheme with lower–upper approximate factorization (LU/AF) subiteration. This flow solver has the same basic structure as the incompressible flow solver of Taylor and Whitfield [22–24] but is adapted for compressible flow with preconditioning and is implemented in primitive variables. It is comprised of an iterative implicit finite-volume scheme, conservative primitive-variable fluxes with third-order MUSCL extrapolation, numerically computed state-vector flux linearizations, and approximate-Newton iteration solved using LU/SGS relaxation.

Iterative implicit schemes are now advantageous for both steady and unsteady flows because they reduce or eliminate linearization and/or factorization errors at each time step, allowing larger time steps and/or improving time accuracy. Iterative implicit relaxation methods were introduced by Chakravarthy [25] and Rai [26] for compressible flow and adapted to incompressible flow by Pan and Chakravarthy [27] and Rogers and Kwak [28], using artificial compressibility. More recently, Whitfield and Taylor et al. [22,29] introduced a *multiple* Newton/relaxation subiteration with both nonlinear and less expensive linear iterations chosen to improve efficiency and robustness at large CFL number. It has subsequently evolved to include multigrid acceleration and scalable parallelism (e.g., Pankajakshan et al. [30]), although the present paper does not address these extensions.

The LU/SGS relaxation is equivalent to a lower–upper approximate factorization (LU/AF) scheme. LU approximate factorization was first proposed by Jameson and Turkel [31] for scalar hyperbolic equations and first implemented for the Euler equations by Buratynski and Caughey [32]. Jameson and Yoon [33] proposed an LU symmetric successive overrelaxation LU/SSOR scheme with multigrid acceleration for the steady two-dimensional Euler equations, and an LU/SGS scheme for approximate Newton iteration of the steady two-dimensional Euler and Navier–Stokes [34] equations. Yoon and Kwak [35] have adapted the LU/SGS scheme of [33] for application to incompressible flows. Many variants of implicit approximate factorization approaches exist in the context of current Euler and Navier–Stokes algorithms. An effort to place many of these in both historical and algorithmic perspective is given by Briley and McDonald [36].

The remainder of this paper is organized as follows: a primitive-variable flux-difference formulation is given in Section 2, and nondimensional flux approximations for the Euler equations are given in Section 3. In Section 4, preconditioned primitive-variable flux-difference approximations that preserve slip-line discontinuities are developed. In Section 5, these preconditioned primitive-variable fluxes are incorporated

into an iterative implicit scheme for the unsteady three-dimensional Navier–Stokes equations. Results for an inviscid shock-tube case computed with the primitive-variable flux but without preconditioning are given in Section 6. Results with preconditioning are given in Section 7 for a flat-plate boundary layer flow at low Mach number, and for highly viscous flow past a cylinder at low Reynolds number, with and without heat transfer. Experimental validations for incompressible and transonic flows are given in Section 8, followed by concluding remarks in Section 9. Appendix A gives nonsingular eigensystems for general dynamic curvilinear coordinates in three dimensions.

2. Characteristic-based primitive-variable flux-difference formulations

Consider the one-dimensional hyperbolic conservation law in conserved variables

$$\frac{\partial \boldsymbol{Q}}{\partial t}+\frac{\partial \boldsymbol{F}(\boldsymbol{Q})}{\partial x}=\frac{\partial \boldsymbol{Q}}{\partial t}+\boldsymbol{A}\frac{\partial \boldsymbol{Q}}{\partial t}=0. \tag{2.1}$$

Here, $\boldsymbol{Q}$ is the solution vector for conservative variables, $\boldsymbol{F}$ is the flux vector, and $\boldsymbol{A}\equiv\partial\boldsymbol{F}/\partial\boldsymbol{Q}$ is the system matrix for $\boldsymbol{Q}$. The scheme

$$\frac{\partial \boldsymbol{Q}_i}{\partial t}+(\mathrm{d}A/\mathrm{d}V)_i(\boldsymbol{F}_{i+1/2}-\boldsymbol{F}_{i-1/2})=0, \tag{2.2}$$

approximates (2.1) on a finite volume $\mathrm{d}V$ with cell interface area $\mathrm{d}A$. Roe's flux approximation [19] is commonly written as

$$\boldsymbol{F}_{i+1/2}=\frac{1}{2}(\boldsymbol{F}_{\mathrm{L}}+\boldsymbol{F}_{\mathrm{R}})-\frac{1}{2}|\tilde{\boldsymbol{A}}|\Delta\boldsymbol{Q}, \tag{2.3}$$

where $|\tilde{\boldsymbol{A}}|\equiv\tilde{\boldsymbol{A}}^{+}-\tilde{\boldsymbol{A}}^{-}$ has positive eigenvalues and can be thought of as a dissipation matrix. Roe's method provides an exact solution to an approximate Riemann problem using an averaged system matrix $\tilde{\boldsymbol{A}}$ constructed to satisfy the flux-difference relationship $\Delta\boldsymbol{F}=\tilde{\boldsymbol{A}}(\boldsymbol{Q}_{\mathrm{R}},\boldsymbol{Q}_{\mathrm{L}})\Delta\boldsymbol{Q}$. Here, $\boldsymbol{Q}_{\mathrm{L}}$ and $\boldsymbol{Q}_{\mathrm{R}}$, are left and right state variables, $\Delta\boldsymbol{F}\equiv\boldsymbol{F}(\boldsymbol{Q}_{\mathrm{R}})-\boldsymbol{F}(\boldsymbol{Q}_{\mathrm{L}})$, $\Delta\boldsymbol{Q}\equiv\boldsymbol{Q}_{\mathrm{R}}-\boldsymbol{Q}_{\mathrm{L}}$, and

$$\tilde{\boldsymbol{A}}^{\pm}=\tilde{\boldsymbol{R}}_{Q}(\tilde{\boldsymbol{\Lambda}}^{\pm})\,\tilde{\boldsymbol{R}}_{Q}^{-1}. \tag{2.4}$$

Changing from $\boldsymbol{Q}$ to a set of primitive variables $\boldsymbol{q}$ gives

$$\frac{\partial}{\partial t}\boldsymbol{Q}(\boldsymbol{q})+\frac{\partial}{\partial x}\boldsymbol{F}[\boldsymbol{Q}(\boldsymbol{q})]=\boldsymbol{M}\frac{\partial \boldsymbol{q}}{\partial t}+\boldsymbol{A}\boldsymbol{M}\frac{\partial \boldsymbol{q}}{\partial x}=0, \tag{2.5}$$

where $\boldsymbol{M}\equiv\partial\boldsymbol{Q}/\partial\boldsymbol{q}$. The system matrix for $\boldsymbol{q}$ is $\boldsymbol{a}=\boldsymbol{M}^{-1}\boldsymbol{A}\boldsymbol{M}$. It is tacitly assumed throughout this paper that $\boldsymbol{q}$ has been chosen so that $\boldsymbol{a}$ has simple eigenvectors; in particular, $\boldsymbol{q}\equiv(\rho,u,v,w,p)^{\mathrm{T}}$ for the Euler equations. Let $\boldsymbol{\Lambda}$ denote the diagonal matrix of eigenvalues of $\boldsymbol{a}$ and let $\boldsymbol{R}_q$ denote a set of right eigenvectors of $\boldsymbol{a}$. Then $\boldsymbol{a}$ can be expressed as $\boldsymbol{a}=\boldsymbol{R}_q\boldsymbol{\Lambda}\boldsymbol{R}_q^{-1}$. Primitive-variable fluxes that recognize discontinuities are given for the finite-volume approximation of (2.5):

$$\frac{\partial \boldsymbol{Q}(\boldsymbol{q}_i)}{\partial t}+(\mathrm{d}A/\mathrm{d}V)_i(\boldsymbol{F}_{i+1/2}-\boldsymbol{F}_{i-1/2})=0. \tag{2.6}$$

Alternatively, the time derivative term can be written in quasilinear form as $\boldsymbol{M}_i\partial\boldsymbol{q}_i/\partial t$. Here, $\boldsymbol{q}_i$ and $\boldsymbol{M}_i$ are volume-averaged values.

The interfacial fluxes are derived for primitive variables using a set of averaged variables $\hat{\boldsymbol{q}}(\boldsymbol{q}_{\mathrm{R}},\boldsymbol{q}_{\mathrm{L}})$, to be defined subsequently. Taking $\Delta\boldsymbol{Q}\approx\tilde{\boldsymbol{M}}\Delta\boldsymbol{q}$ allows (2.3) to be written in an especially simple form:

$$\boldsymbol{F}_{i+1/2} = \frac{1}{2}(\boldsymbol{F}_{\mathrm{L}} + \boldsymbol{F}_{\mathrm{R}}) - \frac{1}{2}\hat{\boldsymbol{M}}|\hat{\boldsymbol{a}}|\Delta\boldsymbol{q}. \tag{2.7}$$

Here, $\Delta\boldsymbol{q} \equiv \boldsymbol{q}_{\mathrm{R}} - \boldsymbol{q}_{\mathrm{L}}$ is the difference of the left and right state variables $\boldsymbol{q}_{\mathrm{L}}$ and $\boldsymbol{q}_{\mathrm{R}}$, across the discontinuity.

3. Nondimensional flux approximations for the Euler equations

3.1. Nondimensional Euler equations in one dimension

Mathematical problem formulations based on dimensional and nondimensional variables are essentially equivalent and do not per se alter their solutions. However, nondimensional variables can be used to extract useful information about relative scales in equations and/or boundary conditions that can guide the preconditioned formulation. The following choice of nondimensional variables was used in [3] to study limiting behavior as $M_{\mathrm{r}} \to 0$ and to suggest a preconditioning that reduced factorization errors. This same nondimensionalization is used here to guide the preconditioning for the characteristics-based primitive-variable flux formulation.

The following reference quantities denoted by a subscript r are used: density, ρ_{r}; velocity, U_{r}; temperature, T_{r}; pressure, $\rho_{\mathrm{r}}U_{\mathrm{r}}^2$; length, L_{r}; time, $L_{\mathrm{r}}/U_{\mathrm{r}}$; energy and enthalpy, h_{r}. With this choice of nondimensional variables, all of the equations given previously in Sections 1 and 2 remain unchanged, except that the variables are now understood to be nondimensional. The nondimensional Euler equations in one dimension are given by (2.1) with $\boldsymbol{Q} = (\rho, \rho u, \rho e_{\mathrm{t}})^{\mathrm{T}}$, and $\boldsymbol{F}(\boldsymbol{Q}) = (\rho u, \rho u^2 + p, \rho u h_{\mathrm{t}})^{\mathrm{T}}$, where ρ is density, u is velocity, p is pressure, e_{t}, is total energy, and h_{t} is total enthalpy. These variables are related by $h_{\mathrm{t}} = e_{\mathrm{t}} + E_c p/\rho$, where E_c is an Eckardt number defined by $E_c = U_{\mathrm{r}}^2/h_{\mathrm{r}}$. These equations are supplemented by an equation of state of the form $\rho = \rho(p, T)$.

For a perfect gas with constant specific heat, $h_{\mathrm{r}} \equiv C_p T_{\mathrm{r}}$, and it follows that $E_c = (\gamma - 1)M_{\mathrm{r}}^2$, where $M_{\mathrm{r}} = u_{\mathrm{r}}/c_{\mathrm{r}}$ is a reference Mach number, $c_{\mathrm{r}}^2 = \gamma R T_{\mathrm{r}}$ is the reference sound speed, $\gamma = C_p/C_{\mathrm{v}}$ is specific heat ratio, and R is the gas constant. The state equation is then given by

$$p = \rho T/\gamma M_{\mathrm{r}}^2 = \rho c^2/\gamma, \quad c^2 = T/M_{\mathrm{r}}^2. \tag{3.1}$$

Other useful relationships are

$$\begin{aligned} h_{\mathrm{t}} &= M_{\mathrm{r}}^2\left[c^2 + (\gamma - 1)\frac{1}{2}u^2\right], \\ e_{\mathrm{t}} &= M_{\mathrm{r}}^2\left[c^2/\gamma + (\gamma - 1)\frac{1}{2}u^2\right]. \end{aligned} \tag{3.2}$$

3.2. Nondimensional eigensystem in one dimension

The eigensystem is easily obtained following a transformation $\boldsymbol{Q}(\boldsymbol{q})$ to the primitive variables $\boldsymbol{q} \equiv (\rho, u, p)^{\mathrm{T}}$. The system matrix for $\boldsymbol{q}$ is

$$\boldsymbol{a} = \boldsymbol{R}_q \boldsymbol{\Lambda} \boldsymbol{R}_q^{-1} = \boldsymbol{M}^{-1}\boldsymbol{A}\boldsymbol{M} = \begin{bmatrix} u & \rho & 0 \\ 0 & u & 1/\rho \\ 0 & \rho c^2 & u \end{bmatrix}. \tag{3.3}$$

The Jacobian for the change of variables is given by

$$\boldsymbol{M} = \frac{\partial \boldsymbol{Q}}{\partial \boldsymbol{q}} = \begin{bmatrix} 1 & 0 & 0 \\ u & \rho & 0 \\ abu^2/2 & ab\rho u & b \end{bmatrix}, \tag{3.4}$$

where $a \equiv \gamma - 1$ and $b \equiv M_r^2$. The eigenvalues of both $\boldsymbol{A}$ and $\boldsymbol{a}$ are $\lambda_i = (u, u + c, u - c)$, and a set of right eigenvectors for $\boldsymbol{a}$ is given by

$$\boldsymbol{R}_q = \begin{bmatrix} 1 & -\rho/c & -\rho/c \\ 0 & -1 & 1 \\ 0 & -\rho c & -\rho c \end{bmatrix}. \tag{3.5}$$

3.3. Averaged variables

It is easily verified that the Roe-averaged variables [17], denoted $\tilde{u}$, $\tilde{h}_t$, $\tilde{\rho}$, $\tilde{c}^2$, satisfy $(\boldsymbol{Q}_R - \boldsymbol{Q}_L) = \tilde{\boldsymbol{M}}(\boldsymbol{q}_R - \boldsymbol{q}_L)$. It therefore follows that Roe's flux-difference property is also satisfied in terms of primitive variables (ρ, u, p) as:

$$\Delta \boldsymbol{F} = \tilde{\boldsymbol{A}} \Delta \boldsymbol{Q} = \tilde{\boldsymbol{A}} \tilde{\boldsymbol{M}} \Delta \boldsymbol{q} = \tilde{\boldsymbol{M}} \tilde{\boldsymbol{a}} \Delta \boldsymbol{q}. \tag{3.6}$$

Consequently, the flux formula (2.7) for (ρ, u, p) variables is equivalent to the Roe flux (2.3) if evaluated using Roe averages. The primitive-variable flux is somewhat simpler for the Euler equations. An alternative flux evaluation is used here, based on an averaged matrix $\hat{\boldsymbol{a}}$ defined using the following averages:

$$\begin{aligned} \hat{\rho} &= \frac{1}{2}(\rho_L + \rho_R), \quad \hat{u} = \frac{1}{2}(u_L + u_R), \\ \hat{h}_t &= \frac{1}{2}(h_{tL} + h_{tR}), \quad \hat{c}^2 = \frac{\hat{h}_t}{M_r^2} - \frac{(\gamma - 1)}{2}\hat{u}^2. \end{aligned} \tag{3.7}$$

Either of these averages preserves the exact solution for a three-dimensional slip-line discontinuity aligned with the grid.

3.4. Other primitive variable choices

It is helpful to recall that $\boldsymbol{Q}$ denotes conservative variables, $\boldsymbol{q} = (\rho, u, p)$ denotes the *primary* set of primitive variables, $\boldsymbol{A} = \partial \boldsymbol{F}/\partial \boldsymbol{Q}$, $\boldsymbol{M} = \partial \boldsymbol{Q}/\partial \boldsymbol{q}$, and $\boldsymbol{a} = \boldsymbol{M}^{-1}\boldsymbol{A}\boldsymbol{M}$. It is also useful to consider a second change of dependent variables from $\boldsymbol{q}$ to some other set $\boldsymbol{w}$. Letting $\boldsymbol{m} \equiv \partial \boldsymbol{q}/\partial \boldsymbol{w}$ and noting that $\boldsymbol{A}\boldsymbol{M}\boldsymbol{m} = \boldsymbol{M}\boldsymbol{a}\boldsymbol{m}$, Eq. (2.5) becomes

$$\boldsymbol{M}\boldsymbol{m}\frac{\partial \boldsymbol{w}}{\partial t} + \frac{\partial}{\partial x}\boldsymbol{F}(\boldsymbol{w}) = \boldsymbol{M}\boldsymbol{m}\frac{\partial \boldsymbol{w}}{\partial t} + \boldsymbol{M}\boldsymbol{a}\boldsymbol{m}\frac{\partial \boldsymbol{w}}{\partial x} = 0. \tag{3.8}$$

The system matrix for $\boldsymbol{w}$ is $\boldsymbol{a}_w = \boldsymbol{m}^{-1}\boldsymbol{a}\boldsymbol{m}$, and the interfacial flux approximation analogous to (2.7) is therefore

$$\boldsymbol{F}_{i+1/2} = \frac{1}{2}(\boldsymbol{F}_L + \boldsymbol{F}_R) - \frac{1}{2}\hat{\boldsymbol{M}}|\hat{\boldsymbol{a}}|\hat{\boldsymbol{m}}\Delta \boldsymbol{w}, \tag{3.9}$$

where $\Delta \boldsymbol{w} \equiv (\boldsymbol{w}_{\mathrm{R}} - \boldsymbol{w}_{\mathrm{L}})$, which is only slightly more complicated than (2.7). It is worth noting that $|\hat{\boldsymbol{a}}|\hat{\boldsymbol{m}} = \hat{\boldsymbol{m}}|\hat{\boldsymbol{a}}_w|$, since $\boldsymbol{a}$ and $\boldsymbol{a}_w$ are similar matrices. The finite-volume approximation can be written as either of

$$\frac{\partial \boldsymbol{Q}(\boldsymbol{w}_i)}{\partial t} + (\mathrm{d}A/\mathrm{d}V)_i(\boldsymbol{F}_{i+1/2} - \boldsymbol{F}_{i-1/2}) = 0, \tag{3.10a}$$

$$(\boldsymbol{M}\boldsymbol{m})_i \frac{\partial \boldsymbol{w}_i}{\partial t} + (\mathrm{d}A/\mathrm{d}V)_i(\boldsymbol{F}_{i+1/2} - \boldsymbol{F}_{i-1/2}) = 0. \tag{3.10b}$$

Computed results are later given for two choices of $\boldsymbol{w}$. A change to $\boldsymbol{w} \equiv (p, u, T)^{\mathrm{T}}$ leads to the following matrix definition:

$$\boldsymbol{m} = \begin{bmatrix} \gamma/c^2 & 0 & -\rho/bc^2 \\ 0 & 1 & 0 \\ 1 & 0 & 0 \end{bmatrix}. \tag{3.11}$$

Alternatively, a change to $\boldsymbol{w} \equiv (\rho, u, T)^{\mathrm{T}}$ gives

$$\boldsymbol{m} = \begin{bmatrix} 1 & 0 & 0 \\ 0 & 1 & 0 \\ c^2/\gamma & 0 & \rho/\gamma b \end{bmatrix}. \tag{3.12}$$

4. Preconditioning for arbitrary Mach number

4.1. Preconditioned formulation in primitive variables

A preconditioning matrix $\boldsymbol{\Gamma}_q$ is introduced into the quasilinear form of (2.6) as follows:

$$\boldsymbol{M}\boldsymbol{\Gamma}_q^{-1}\frac{\partial \boldsymbol{q}}{\partial t} + \frac{\partial}{\partial x}\boldsymbol{F}(\boldsymbol{q}) = 0. \tag{4.1}$$

This can be expanded and rewritten as

$$\frac{\partial \boldsymbol{q}}{\partial t} + \boldsymbol{a}_\Gamma \frac{\partial \boldsymbol{q}}{\partial x} = 0, \tag{4.2}$$

where $\boldsymbol{a}_\Gamma \equiv \boldsymbol{\Gamma}_q \boldsymbol{a}$ is the system matrix for the preconditioned formulation. An eigensystem for $\boldsymbol{a}_\Gamma$ will be needed to develop characteristic-based flux approximations. Let $\boldsymbol{\Lambda}_\Gamma$ denote the diagonal matrix of eigenvalues of $\boldsymbol{a}_\Gamma$ and let $\boldsymbol{R}_\Gamma$ denote a set of right eigenvectors of $\boldsymbol{a}_\Gamma$. Then $\boldsymbol{a}_\Gamma$ can be expressed as $\boldsymbol{a}_\Gamma = \boldsymbol{R}_\Gamma \boldsymbol{\Lambda}_\Gamma \boldsymbol{R}_\Gamma^{-1}$.

Note that it is not necessary to define $\boldsymbol{A}_\Gamma = \boldsymbol{M}\boldsymbol{a}_\Gamma\boldsymbol{M}^{-1}$ or its eigenvectors, since the form of the flux follows directly from (4.2) rewritten as:

$$\boldsymbol{M}\boldsymbol{\Gamma}_q^{-1}\frac{\partial \boldsymbol{q}}{\partial t} + \boldsymbol{M}\boldsymbol{\Gamma}_q^{-1}\boldsymbol{a}_\Gamma \frac{\partial \boldsymbol{q}}{\partial x} = 0. \tag{4.3}$$

Introducing averaged variables $\hat{\boldsymbol{q}}$, the flux approximation analogous to (2.7) but including the preconditioning matrix $\hat{\boldsymbol{\Gamma}}_q$ is

$$\boldsymbol{F}_{i+1/2} = \frac{1}{2}(\boldsymbol{F}_{\mathrm{L}} + \boldsymbol{F}_{\mathrm{R}}) - \frac{1}{2}\hat{\boldsymbol{M}}\hat{\boldsymbol{\Gamma}}_q^{-1}|\hat{\boldsymbol{\Gamma}}_q\hat{\boldsymbol{a}}|\Delta\boldsymbol{q} \tag{4.4}$$

and the finite-volume approximation analogous to (2.6) is

$$(\boldsymbol{M}\boldsymbol{\Gamma}_q^{-1})_i \frac{\partial \boldsymbol{q}_i}{\partial t} + (\mathrm{d}A/\mathrm{d}V)_i(\boldsymbol{F}_{i+1/2} - \boldsymbol{F}_{i-1/2}) = 0, \tag{4.5}$$

where $(\boldsymbol{M}\boldsymbol{\Gamma}_q^{-1})_i$ and $\boldsymbol{q}_i$ are volume-averaged values. Selection of a preconditioning matrix for $\hat{\boldsymbol{\Gamma}}_q$ for (4.4) is straight-forward.

4.2. Other primitive variable choices

To change variables from $\boldsymbol{q} = (\rho, u, p)$ to $\boldsymbol{w}$, the above development can be repeated after replacing (4.2) with a preconditioned form of (3.10a) and (3.10b):

$$\frac{\partial \boldsymbol{w}}{\partial t} + \boldsymbol{\Gamma}_w \boldsymbol{a}_w \frac{\partial \boldsymbol{w}}{\partial x} = 0. \tag{4.6}$$

This leads to

$$\boldsymbol{F}_{i+1/2} = \frac{1}{2}(\boldsymbol{F}_{\mathrm{L}} + \boldsymbol{F}_{\mathrm{R}}) - \frac{1}{2}\hat{\boldsymbol{M}}\hat{\boldsymbol{m}}\hat{\boldsymbol{\Gamma}}_w^{-1}|\hat{\boldsymbol{\Gamma}}_w\hat{\boldsymbol{a}}_w|\Delta\boldsymbol{w}, \tag{4.7}$$

$$(\boldsymbol{M}\boldsymbol{m}\boldsymbol{\Gamma}_w^{-1})_i \frac{\partial \boldsymbol{w}_i}{\partial t} + (\mathrm{d}A_i/V)(\boldsymbol{F}_{i+1/2} - \boldsymbol{F}_{i-1/2}) = 0. \tag{4.8}$$

Note, however, that this requires an eigensystem for $\hat{\boldsymbol{\Gamma}}_w\hat{\boldsymbol{m}}^{-1}\hat{\boldsymbol{a}}\hat{\boldsymbol{m}}$. A simpler alternative is to use

$$\boldsymbol{F}_{i+1/2} = \frac{1}{2}(\boldsymbol{F}_{\mathrm{L}} + \boldsymbol{F}_{\mathrm{R}}) - \frac{1}{2}\hat{\boldsymbol{M}}\hat{\boldsymbol{\Gamma}}_q^{-1}|\hat{\boldsymbol{\Gamma}}_q\hat{\boldsymbol{a}}|\hat{\boldsymbol{m}}\Delta\boldsymbol{w}, \tag{4.9}$$

$$(\boldsymbol{M}\boldsymbol{\Gamma}_q^{-1}\boldsymbol{m})_i \frac{\partial \boldsymbol{w}_i}{\partial t} + (\mathrm{d}A_i/V)(\boldsymbol{F}_{i+1/2} - \boldsymbol{F}_{i-1/2}) = 0, \tag{4.10}$$

instead of (4.4) and (4.5). This alternative only requires the preconditioning and eigensystem for (ρ, u, p) variables $(\hat{\boldsymbol{\Gamma}}_q, \hat{\boldsymbol{a}})$. The relationship of (4.9) to (4.4) is analogous to that of the flux (3.9) to (2.7).

4.3. Preconditioning matrix for $\boldsymbol{q} = (\rho, u, p)^T$

A simple but effective preconditioning for implicit approximate factorization algorithms replaces $\hat{\boldsymbol{\Gamma}}_q$ by a diagonal matrix of constants that depend only on M_{r}, as in [3]. Specifically, let $\hat{\boldsymbol{\Gamma}}_q = \mathrm{diag}[1, 1, \beta(M_{\mathrm{r}})]$. The system matrix becomes

$$\boldsymbol{\Gamma}\hat{\boldsymbol{a}} = \begin{bmatrix} \hat{u} & \hat{\rho} & 0 \\ 0 & \hat{u} & 1/\hat{\rho} \\ 0 & \beta\hat{\rho}\hat{c}^2 & \beta\hat{u} \end{bmatrix}, \tag{4.11}$$

where $\beta^{\pm} \equiv (1 \pm \beta)/2$ and $\hat{\sigma}^2 \equiv (\hat{u}\beta^-)^2 + \beta\hat{c}^2$, and its eigenvalues are

$$\hat{\lambda} = \hat{u}, \quad \hat{u}\beta^+ \pm \hat{\sigma}. \tag{4.12}$$

The choice $\beta = 1$ recovers the unpreconditioned formulation. The following choice for β is sufficient to provide well-behaved eigenvalues in terms of nondimensional variables u and T, which are assumed to be $\mathrm{O}(1)$:

$$\beta(M_r) = \begin{cases} M_r^2 & (M_r < 1), \\ 1 & (M_r \geqslant 1), \end{cases} \tag{4.13}$$

where $M_r(u_r, T_r) = u_r/\sqrt{\gamma R T_r}$. Although dimensional reference quantities can be chosen arbitrarily to arrive at nondimensional equations, the specific values chosen are obviously important when preconditioning is used. In general, u_r and T_r should have values representative of global flow properties for each particular flow case. For external flows, the freestream values of u_r and T_r were used for all cases considered here. A shock-tube case is considered in which the flow is initially at rest, and much of the flow remains at rest (zero local velocity and Mach number), while the shock itself propagates at supersonic speed. In this case, the reference variables were chosen so that $M_r = 1$. It is possible that more complex problems will require a nonconstant definitions of β that depend on local variables.

4.4. Preservation of slip-line discontinuities

The capturing of a slip-line discontinuity aligned with a solid boundary is illustrated here for a three-dimensional Cartesian grid with y normal to the boundary. The required eigensystem for $\boldsymbol{\Gamma}\hat{\boldsymbol{a}}$ for general three-dimensional dynamic curvilinear coordinate systems are given in Appendix A. The slip surface may have discontinuous tangential shear velocities u, w and is characterized by the conditions $v = \Delta v = \Delta p = 0$. The discontinuity is captured if the following vector embedded in the dissipation matrix is zero:

$$|\boldsymbol{\Gamma}|\boldsymbol{R}_q^{-1}\Delta\boldsymbol{q} = \begin{bmatrix} -v\Delta w \\ v\Delta\rho + 2\rho v^2 \frac{\beta^-}{\beta c^2}\Delta v \frac{v}{\beta c^2}\Delta p \\ -\frac{v\beta^- - \sigma}{2\sigma}(v\beta^+ + \sigma)\Delta v + \frac{1}{2\rho\sigma}(v\beta^+ + \sigma)\Delta p \\ -\frac{v\beta^- + \sigma}{2\sigma}(v\beta^+ - \sigma)\Delta v + \frac{1}{2\rho\sigma}(v\beta^+ - \sigma)\Delta p \end{bmatrix}, \tag{4.14}$$

where $\sigma^2 \equiv (v\beta^-)^2 + \beta c^2$. The first three components are zero if v is zero, and the last two are zero if $\Delta v = \Delta p = 0$. Consequently, the discontinuity is captured with or without preconditioning, and independent of the averaging used, provided that $\hat{v} = 0$. This property will be demonstrated in subsequent computed results.

4.5. Relationship to previous preconditionings

Turkel [2,9] has reviewed numerous approaches to preconditioning. Of particular interest here is Turkel's [2] general preconditioning matrix $\boldsymbol{P}_0$ defined relative to entropy variables $\boldsymbol{w_0}$, but also given as $\boldsymbol{P}_T$ for $\boldsymbol{w} = (\boldsymbol{p}, \boldsymbol{u}, \boldsymbol{T})^T$. Turkel shows that the matrix $\boldsymbol{P}_T$, which depends on three parameters (β, α, δ), reduces to preconditionings of Turkel et al. [2,9] ($\delta = 0$), Choi and Merkle [11] ($\alpha = 0, \delta = 1$), and Weiss and Smith [12] ($\alpha = 0, \delta = 0$). In the present notation, the preconditioning matrix $\boldsymbol{\Gamma}_w$ is related to Turkel's $\boldsymbol{P}_T$ by

$$\boldsymbol{\Gamma}_w^{-1} \leftarrow \boldsymbol{MmP}_T^{-1}. \tag{4.15}$$

All of these preconditioning matrices have parameters that depend on local flow variables, with some type of limiter to avoid singularities at stagnation points. In this regard, it is of interest to compare the present preconditioned eigenvalues with those of two previous methods. The acoustic eigenvalues given by Choi and Merkle [6] for their inviscid preconditioning can be written as

$$\frac{u_l}{2}(1 + M^2) \pm \sqrt{\frac{u_l^2}{4}(1 - M^2)^2 + u_l^2}, \tag{4.16}$$

where u_l, denotes the local dimensional velocity, and M is local Mach number. Recalling that $\hat{c}^2 = \hat{T}/M_r^2$, the present eigenvalues (4.12) can be written as

$$\frac{\hat{u}}{2}(1+M_r^2) \pm \sqrt{\frac{\hat{u}^2}{4}(1-M_r^2)^2 + \hat{T}}. \tag{4.17}$$

Note that the nondimensional, local, averaged variables $\hat{u}$ and $\hat{T}$ are both O(1) quantities as long as the reference quantities U_r and T_r are indicative of the global flow behavior, thus guaranteeing that the eigenvalues are well behaved as $M_r \to 0$. Since $u_l \to 0$ at stagnation points, (4.16) is degenerate, whereas (4.17) reduces to $\pm\sqrt{\hat{T}}$ as $\hat{u} \to 0$. The eigenvalue behavior is thus substantially different near stagnation points, even though the forms of the diagonal preconditioning matrices are similar.

Similarly, the acoustic eigenvalues of Weiss and Smith [12] can be written as

$$\frac{u_l}{2}(1+\beta U_{\mathrm{ref}}^2) \pm \sqrt{\frac{u_l^2}{4}(1-\beta U_{\mathrm{ref}}^2)^2 + U_{\mathrm{ref}}^2}, \tag{4.18}$$

where $\beta = (\rho_p + \rho_T/\rho C_p)$. For an ideal gas, $U_{\mathrm{ref}}(\epsilon, |u_l|, c_l)$ is a local velocity limited by the local sound speed c_l, and ϵc_l. Both inviscid ($\epsilon \sim 10^{-5}$) and viscous ($\nu/\Delta x$) limiters are used for U_{ref}. When $\rho = \rho(T)$ or for an incompressible fluid, $U_{\mathrm{ref}}(\epsilon, |u_l|, U_{\max})$ depends on the maximum velocity in the field $U_{\max}$. At stagnation points, these eigenvalues are controlled by the limiter, reducing to either $\pm\epsilon c_l$ or $\pm\epsilon U_{\max}$, both relatively small values.

Weiss and Smith [12] also use a preconditioned modification of Roe's flux-difference scheme [19] in terms of $\boldsymbol{w} = (p, u, T)^T$ variables. Their preconditioning can be related to the present notation by

$$\boldsymbol{\Gamma}_w^{-1} = \boldsymbol{K}^{-1}(\boldsymbol{KMm})_\Theta. \tag{4.19}$$

Here, $\boldsymbol{K}$ is the matrix that transforms the Euler equations to nonconservative form, and the single occurrence of $\partial\rho/\partial p$ in the matrix $\boldsymbol{KMm}$ has been replaced by a preconditioning function $\partial\rho/\partial p \leftarrow \Theta \equiv [U_{\mathrm{ref}}^{-2} - \rho_T/\rho C_p]$. The final flux formula and finite volume scheme can be expressed as

$$\boldsymbol{F}_{i+1/2} = \frac{1}{2}(\boldsymbol{F}_L + \boldsymbol{F}_R) - \frac{1}{2}\boldsymbol{\Gamma}_w^{-1}|\boldsymbol{\Gamma}_w\boldsymbol{Mam}|\Delta\boldsymbol{w}, \tag{4.20a}$$

$$(\boldsymbol{\Gamma}_w^{-1})_i \frac{\partial \boldsymbol{w}_i}{\partial \boldsymbol{t}} + (\mathrm{d}A/V)_i(\boldsymbol{F}_{i+1/2} - \boldsymbol{F}_{i-1/2}) = 0. \tag{4.20b}$$

These formulas can be compared with (4.4) and (4.5) and (4.7)–(4.10).

5. Iterative implicit unsteady flow solver

5.1. Upwind finite-volume scheme

The three-dimensional unsteady compressible Reynolds-averaged Navier–Stokes equations are solved by introducing preconditioning, when needed, to facilitate iterative solution at each physical time step. A cell-centered finite-volume scheme for a dynamic curvilinear coordinate system can be written as

$$(\boldsymbol{M}\boldsymbol{\Gamma}_q^{-1})_V \frac{\partial \boldsymbol{q}}{\partial \boldsymbol{\tau}} = -[\boldsymbol{\delta}_i(\boldsymbol{F} - \boldsymbol{F}_v) + \boldsymbol{\delta}_j(\boldsymbol{G} - \boldsymbol{G}_v) + \boldsymbol{\delta}_k(\boldsymbol{H} - \boldsymbol{H}_v)] = -\boldsymbol{R}(q). \tag{5.1}$$

Here, $\boldsymbol{R}(q)$ is the steady residual vector, $\boldsymbol{q} = J(\rho, u, v, w, p)^{\mathrm{T}}$ is the solution vector, and J is the Jacobian of the inverse coordinate transformation. The inviscid flux vectors are $\boldsymbol{F}$, $\boldsymbol{G}$, $\boldsymbol{H}$, the viscous flux components including modeled turbulent stresses are $\boldsymbol{F}_v$, $\boldsymbol{G}_v$, $\boldsymbol{H}_v$, and τ is time. The central difference operators are defined as in $\delta_i(\cdot) \equiv (\cdot)_{i+1/2} - (\cdot)_{i-1/2}$ for each i, j, k direction, corresponding to the respective curvilinear ξ, η, and ζ coordinate directions. A subscript $(\cdot)_V$ denotes a volume-averaged quantity. Detailed definitions are given in [23].

5.2. Numerical fluxes

The inviscid flux vectors at each cell face are obtained using the numerical flux formulas (2.14) or (4.4), with van Leer's MUSCL extrapolation of left and right state vectors, $\boldsymbol{q}_{\mathrm{R}}$ and $\boldsymbol{q}_{\mathrm{L}}$, as implemented in the third-order form of Anderson et al. [37], and with a van Leer limiter. The flux approximation for the i direction is as in (2.7), or (4.4) with preconditioning. Analogous definitions for the j and k direction fluxes are obtained by replacing $[i, \boldsymbol{F}, \boldsymbol{a}]$ by $[j, \boldsymbol{G}, \boldsymbol{b}]$ or $[k, \boldsymbol{H}, \boldsymbol{c}]$, and using corresponding eigensystems to define $\boldsymbol{b}^{\pm}$ and $\boldsymbol{c}^{\pm}$. Details and nonsingular eigensystems that use metric information from only one direction are given in Appendix A.

5.3. Iterative implicit unsteady algorithm

An iterative implicit nonlinear scheme for solving (5.1) is given by

$$(\boldsymbol{M}\boldsymbol{\Gamma}_q^{-1})_V^s \Delta \boldsymbol{q}^{n,s+1}/\Delta\boldsymbol{\tau} = -\boldsymbol{R}(\boldsymbol{q}^{n+1,s+1}), \tag{5.2}$$

where $\Delta(\cdot)^n \equiv (\cdot)^{n+1} - (\cdot)^n$, and $s = 0, 1, \ldots$ is an iteration index. For the nonlinear spatial residual, a discrete linearization about a previous iteration state $\boldsymbol{q}^{n+1,s}$ is written in the form

$$\boldsymbol{R}(\boldsymbol{q}^{n+1,s+1}) = \boldsymbol{R}(\boldsymbol{q}^{n+1,s}) + \mathscr{L}^{n+1,s}(\Delta_s \boldsymbol{q}^{n+1,s}) + \mathrm{O}(\Delta_s \boldsymbol{q}^{n+1,s})^2, \tag{5.3}$$

where $\Delta_s(\cdot) \equiv (\cdot)^{s+1} - (\cdot)^s$, and $\mathscr{L}^{n+1,s}(\cdot)$ is a linear spatial difference operator made up of flux derivatives to be defined subsequently. This leads to the following iterative linearized implicit scheme:

$$[\Delta\tau^{-1}(\boldsymbol{M}\boldsymbol{\Gamma}_q^{-1})_V^s + \mathscr{L}^{n+1,s}(\cdot)](\Delta_s \boldsymbol{q}^{n+1,s}) = -\boldsymbol{R}_{\mathrm{U}}(\boldsymbol{q}^{n+1,s}). \tag{5.4}$$

Here, the *physical* unsteady residual $\boldsymbol{R}_{\mathrm{U}}$ is defined as either

$$\boldsymbol{R}_{\mathrm{U}}(\boldsymbol{q}^{n+1,s}) = [\Delta\tau^{-1}\boldsymbol{M}_V^{n+1}(\boldsymbol{q}^{n+1,s} - \boldsymbol{q}^n) + \boldsymbol{R}(\boldsymbol{q}^{n+1,s})] \tag{5.5a}$$

or using the conservative time derivative form

$$\boldsymbol{R}_{\mathrm{U}}(\boldsymbol{q}^{n+1,s}) = [\Delta\tau^{-1}[\boldsymbol{Q}(\boldsymbol{q}^{n+1,s}) - \boldsymbol{Q}(\boldsymbol{q}^n)] + \boldsymbol{R}(\boldsymbol{q}^{n+1,s})]. \tag{5.5b}$$

The converged solution then satisfies the physical unsteady approximation $\boldsymbol{R}_{\mathrm{U}} = 0$ with or without preconditioning. The first-order time accurate approximations in (5.5a) and (5.5b) were used for all present calculations, but these are easily modified for higher-order backward-Euler time approximations.

5.4. Numerical state-vector flux linearization

The flux linearization matrices are computed numerically, as proposed by Whitfield and Taylor [22,23]. The authors have found that accurate linearization matrices provide better stability and iterative convergence rates than more approximate flux Jacobians. Whitfield and Taylor [24] also proposed a new numerical flux linearization in which the numerical fluxes (i.e., $\boldsymbol{F}_{i+1/2}$) are differentiated with respect to the left

and right solution-variable state vectors $\boldsymbol{q}_{\mathrm{R}}$ and $\boldsymbol{q}_{\mathrm{L}}$, instead of the nodal values $\boldsymbol{q}_i$, and $\boldsymbol{q}_{i+1}$. This technique is more economical, avoids the issue of whether to omit derivatives with respect to $\boldsymbol{q}_{i+2}$ in high-order fluxes, and also seems to perform well in practical calculations. These numerical *state-vector flux linearizations* are defined [24] by

$$\hat{\boldsymbol{A}}_i^+ = \frac{\partial \boldsymbol{F}_{i+1/2}}{\partial \boldsymbol{q}_{i+1/2}^{\mathrm{L}}}, \quad \hat{\boldsymbol{A}}_i^- = \frac{\partial \boldsymbol{F}_{i-1/2}}{\partial \boldsymbol{q}_{i-1/2}^{\mathrm{R}}} \tag{5.6}$$

and the kth column of each matrix is evaluated as in

$$\hat{\boldsymbol{A}}_i^+ = [\boldsymbol{F}_{i+1/2}(\boldsymbol{q}_{i+1/2}^{\mathrm{R}}, \boldsymbol{q}_{i+1/2}^{\mathrm{L}} + h\boldsymbol{e}_k) - \boldsymbol{F}_{i+1/2}(\boldsymbol{q}_{i+1/2}^{\mathrm{R}}, \boldsymbol{q}_{i+1/2}^{\mathrm{L}})]/h, \tag{5.7}$$

where $\boldsymbol{e}_k$ is the kth unit vector and $h \approx \sqrt{\text{machine zero}}$. Analogous definitions apply to $\hat{\boldsymbol{B}}_j$ and $\hat{\boldsymbol{C}}_j$. The linearized flux derivative operative $\mathscr{L}^n(\cdot)$ can now be defined as

$$\begin{aligned}\mathscr{L}^n(\cdot) = {} & -\hat{\boldsymbol{A}}_{i-1}^+(\cdot)_{i-1} + (\hat{\boldsymbol{A}}_i^+ - \hat{\boldsymbol{A}}_i^-)(\cdot)_i + \hat{\boldsymbol{A}}_{i+1}^-(\cdot)_{i+1} - \hat{\boldsymbol{B}}_{j-1}^+(\cdot)_{j-1} + (\hat{\boldsymbol{B}}_j^+ - \hat{\boldsymbol{B}}_j^-)(\cdot)_j + \hat{\boldsymbol{B}}_{j+1}^-(\cdot)_{j+1} \\ & - \hat{\boldsymbol{C}}_{k-1}^+(\cdot)_{k-1} + (\hat{\boldsymbol{C}}_k^+ - \hat{\boldsymbol{C}}_k^-)(\cdot)_k + \hat{\boldsymbol{C}}_{k+1}^-(\cdot)_{k+1}.\end{aligned} \tag{5.8}$$

5.5. Solution of the linearized scheme using LU/SGS relaxation

The solution of the linearized scheme (5.4) for $\Delta_s \boldsymbol{q}^{n+1,s}$ is obtained by lower–upper Symmetric Gauss–Seidel (LU/SGS) relaxation. Introducing a second subiteration index m and appropriate definitions for the matrix $\boldsymbol{D}$ and operators $\mathscr{L}_1$, and $\mathscr{L}_2$, the LU/SGS scheme can be written as

$$\begin{aligned}&[\boldsymbol{D}^{n+1,s} + \mathscr{L}_1^{n+1,s}(\cdot)](\Delta_s \boldsymbol{q}^{n+1,s})^* + \mathscr{L}_2^{n+1,s}(\Delta_s \boldsymbol{q}^{n+1,s})^m = \boldsymbol{R}_{\mathrm{U}}(\boldsymbol{q}^{n+1,s}), \\ &[\boldsymbol{D}^{n+1,s} + \mathscr{L}_2^{n+1,s}(\cdot)](\Delta_s \boldsymbol{q}^{n+1,s})^{m+1} + \mathscr{L}_1^{n+1,s}(\Delta_s \boldsymbol{q}^{n+1,s})^* = \boldsymbol{R}_{\mathrm{U}}(\boldsymbol{q}^{n+1,s}).\end{aligned} \tag{5.9}$$

The definitions of $\boldsymbol{D}$, $\mathscr{L}_1$, and $\mathscr{L}_2$ for the LU/SGS scheme are:

$$\boldsymbol{D}(\cdot) = [\Delta\tau^{-1}(\boldsymbol{M}\boldsymbol{\Gamma}_q^{-1})_V + (\hat{\boldsymbol{A}}_i^+ - \hat{\boldsymbol{A}}_i^-) + (\hat{\boldsymbol{B}}_j^+ - \hat{\boldsymbol{B}}_j^-) + (\hat{\boldsymbol{C}}_k^+ - \hat{\boldsymbol{C}}_k^-)](\cdot)_{i,j,k}, \tag{5.10a}$$

$$\mathscr{L}_1(\cdot) = -\hat{\boldsymbol{A}}_{i-1}^+(\cdot)_{i-1} - \hat{\boldsymbol{B}}_{j-1}^+(\cdot)_{j-1} - \hat{\boldsymbol{C}}_{k-1}^+(\cdot)_{k-1}, \tag{5.10b}$$

$$\mathscr{L}_2(\cdot) = +\hat{\boldsymbol{A}}_{i+1}^-(\cdot)_{i+1} + \hat{\boldsymbol{B}}_{j+1}^-(\cdot)_{j+1} + \hat{\boldsymbol{C}}_{k+1}^-(\cdot)_{k+1}, \tag{5.10c}$$

which satisfy the following consistency relationship:

$$\boldsymbol{D}(\cdot) + \mathscr{L}_1(\cdot) + \mathscr{L}_2(\cdot) = \Delta\tau^{-1}(\boldsymbol{M}\boldsymbol{\Gamma}_q^{-1})_V(\cdot) + \mathscr{L}(\cdot). \tag{5.11}$$

The solution is updated as in $\boldsymbol{q}^{n+1,s+1} \leftarrow \boldsymbol{q}^{n+1,s} + \Delta_s \boldsymbol{q}^{n+1,s}$ following a specified number of LU/SGS iterations. The quantity $\Delta_s \boldsymbol{q}^{n+1,s}$ approaches zero as the s-iteration converges, giving a solution to $\boldsymbol{R}_{\mathrm{U}}(\boldsymbol{q}^{n+1}) = 0$.

6. Inviscid shock-tube results without preconditioning

Computed results are given for a one-dimensional inviscid shock-tube problem solved in the region $(0 \leqslant x \leqslant 1)$. The initial discontinuity is located at the center of the region $x = 0.5$, and the initial left and right states are

$$\begin{aligned} \boldsymbol{q}_{\mathrm{L}}(\rho,u,p) &= (1,0,\gamma^{-1})^{\mathrm{T}}, \\ \boldsymbol{q}_{\mathrm{R}}(\rho,u,p) &= (1/8,0,\gamma^{-1}/10)^{\mathrm{T}}. \end{aligned} \tag{6.1}$$

All solutions were computed using the third-order inviscid flux, with 15 Newton iterations and 15 linear subiterations at each time step. Convergence of the unsteady residual to machine zero required only 10 Newton iterations, although 15 were computed. The computed profiles for the shock propagation are shown at a nondimensional time of 0.17, after 1000 steps with $\Delta t = 0.00017$, which corresponds to CFL = 2. The uniform grid has 200 points with spacing $\Delta x = 0.005$.

In Fig. 1, profiles computed with the present primitive-variable scheme using $\boldsymbol{q} = (\rho,u,p)^{\mathrm{T}}$ variables with fluxes evaluated using both algebraic and Roe averages are compared with the exact solution. These profiles are compared with the exact solution and also with profiles computed with an existing compressible code [38] that uses conservative variables and the standard Roe flux with $\tilde{\boldsymbol{A}}(\boldsymbol{Q}_{\mathrm{L}},\boldsymbol{Q}_{\mathrm{R}})$. All of the computed profiles in Fig. 1 are almost identical, and all agree reasonably well with the exact solution. These results serve to demonstrate that the primitive-variable flux with algebraic averages has accuracy similar to those obtained with Roe averages, as well as the standard Roe flux. Recall that the $\boldsymbol{q}$ variables and algebraic averages offer the least complexity.

Another comparison is shown in Fig. 2 for the primitive-variable fluxes based on each of the variable choices $\boldsymbol{q} = (\rho,u,p)^{\mathrm{T}}$, $\boldsymbol{w}_1 = (\rho,u,T)^{\mathrm{T}}$, and $\boldsymbol{w}_2 = (p,u,T)^{\mathrm{T}}$, using algebraic averages and using quasilinear time derivatives in the unsteady residual, as in (5.5a). Again, the computed profiles are almost identical, suggesting that the choice of primitive variables is not important for this particular problem. Finally, in Fig. 3, solutions for these same three variable choices are given for algebraic averages and conservative time derivatives as in (5.5b). Again, there is little difference for this test problem.

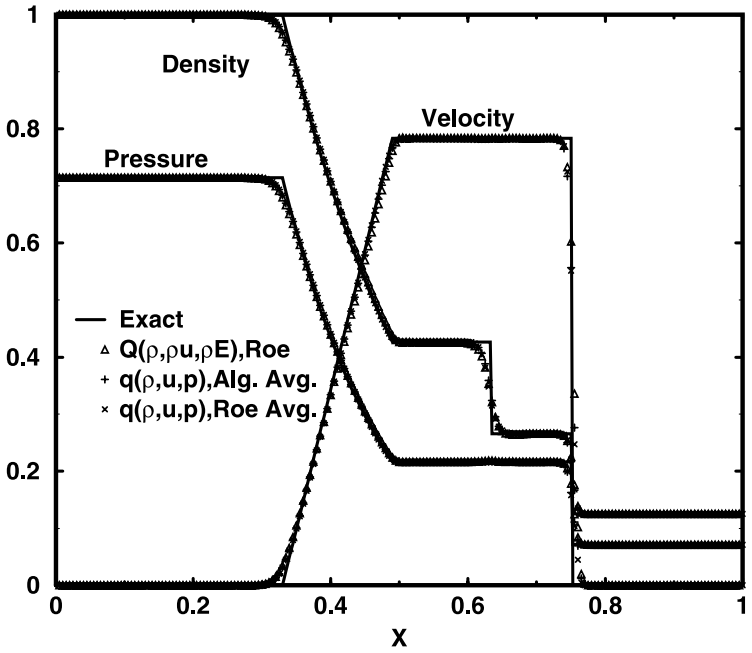

Fig. 1. Comparison of exact profiles for the shock-tube problem with profiles computed using the standard Roe flux and using the present scheme in (ρ,u,p) variables with both algebraic and Roe averages ($\beta = M_{\mathrm{r}} = 1$).

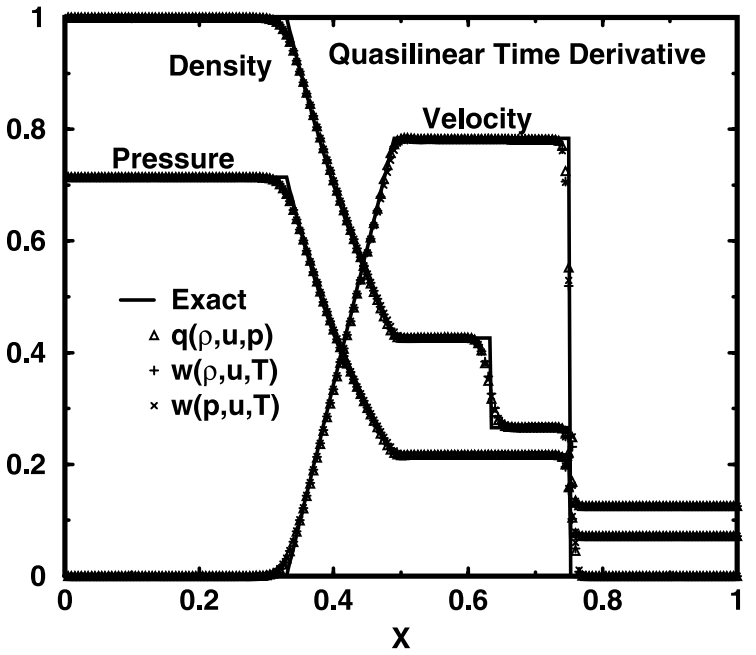

Fig. 2. Comparison of exact profiles for the shock-tube problem with profiles computed with three primitive variable choices and with quasilinear time derivatives in unsteady residual ($\beta = M_r = 1$).

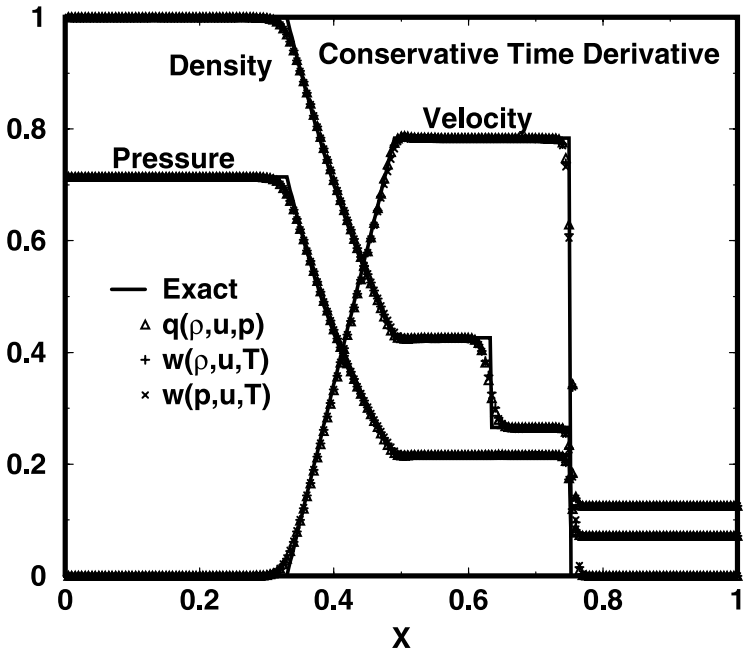

Fig. 3. Comparison of exact profiles for the shock-tube problem with profiles computed with three primitive variable choices and with conservative time derivatives in unsteady residual ($\beta = M_r = 1$).

It is worth noting that none of the present solutions required any type of entropy modification to prevent rarefaction shocks. Godunov's method with Roe's Riemann solver has required an entropy fix for a similar problem (cf. Toro [18]). No effort has been made to explain this, however, and it is quite possible that shock-capturing anomalies would be encountered in other cases using the present scheme. Many shock-capturing anomalies have been reported for different algorithms and flow cases (cf. Quirk [39]), including the "carbuncle phenomenon" for blunt-body flows. Liou [40] has recently studied shock instability in shock-capturing schemes and suggested a method for developing shock-stable schemes.

7. Test cases with preconditioning

7.1. Viscous resolution for laminar boundary layer flow

It was suggested in Section 1 that a conservative characteristic-based flux formulation is advantageous for high resolution of boundary-layer regions. This issue is examined here for a laminar boundary-layer flow past a flat plate with a rectangular (71×21) grid with 50 uniform intervals with spacing $\Delta x = 0.02$ along the unit length of the plate. The normal-direction grid is distributed to provide increased resolution near the wall, with minimum spacing of $\Delta y = 10^{-4}$ at the wall. The grid extends to a distance of 5 lengths upstream and downstream of the leading edge, and 5 lengths to the outer boundary. The freestream and reference Mach numbers are 10^{-3} for all flat-plate solutions.

In Fig. 4, three solutions are shown for the velocity profile at midchord, each computed with the present scheme using $\boldsymbol{q}$ variables and algebraic averages for fluxes. The first two solutions are inviscid solutions

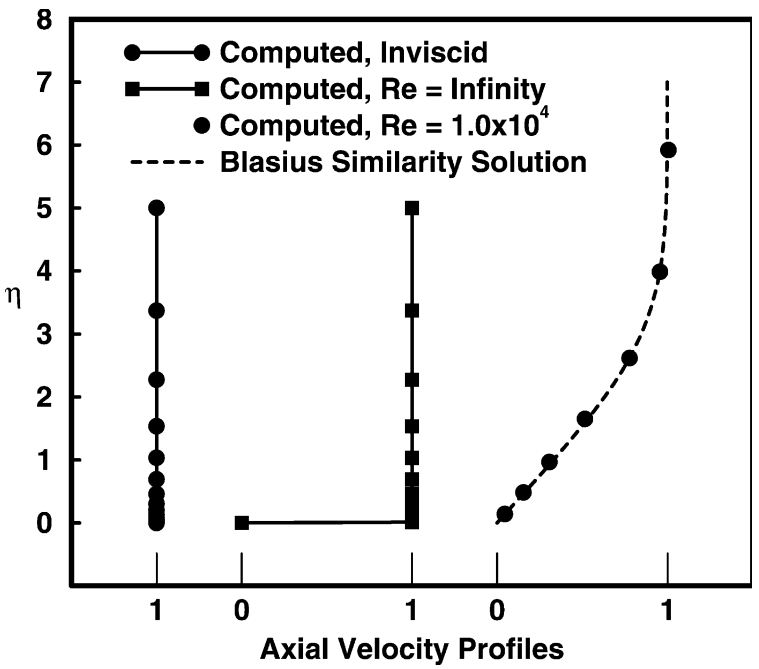

Fig. 4. Computed midchord velocity profiles for flow past a flat plate: Inviscid flow with slip and no-slip conditions, and viscous flow at $Re = 10^4$ compared with the Blasius solution ($M_r = 10^{-3}$).

computed for zero viscosity. One is a uniform flow with inviscid slip condition at the wall boundary, while the other imposes a zero velocity no-slip condition. The exact solution for the latter solution is an inviscid slip-line discontinuity located at the wall, and this is the limiting solution for infinite Reynolds number. Both of these solutions reproduce the corresponding exact solution. As the Reynolds number is reduced, the viscous terms cause the vortex sheet to diffuse and form a boundary layer along the plate. The third solution shows the velocity profile for $Re = 10^4$, which agrees very well with the Blasius similarity solution, even with only six grid intervals in the boundary layer.

The minimum resolution required for this particular flow case is explored further in Figs. 5 and 6, which show the influence of different grid spacings normal to the wall both on the midchord velocity profile, and on the axial distribution of skin friction coefficient $C_f = \tau_w/\frac{1}{2}\rho_0 U_0^2$. Although the leading-edge region is not well resolved for these grids, it can be seen in Figs. 5 and 6 that with as few as five points in the boundary layer at midchord, both the velocity profile and the skin friction distribution are reasonably well-predicted downstream of the leading edge. The large error in C_f caused by poor resolution near the leading edge is also evident. The good agreement with only seven points in the midchord boundary layer is noteworthy, and a possible explanation is the flux property that preserves slip-line discontinuities.

7.2. Laminar and turbulent flow past a flat plate at low Mach number

The influence of Mach number on solutions computed using the preconditioned formulation is explored here for both laminar and turbulent flow past a flat plate at low Mach numbers. Recall that if adiabatic wall conditions are used, these compressible perfect-gas solutions closely approximate an incompressible flow (cf. [3]). The turbulent solutions use a $q-\omega$ turbulence model [41,42], with wall spacing of $y^+ \approx 1$ at the wall. These solutions are computed with the present scheme using $\boldsymbol{q}$ variables

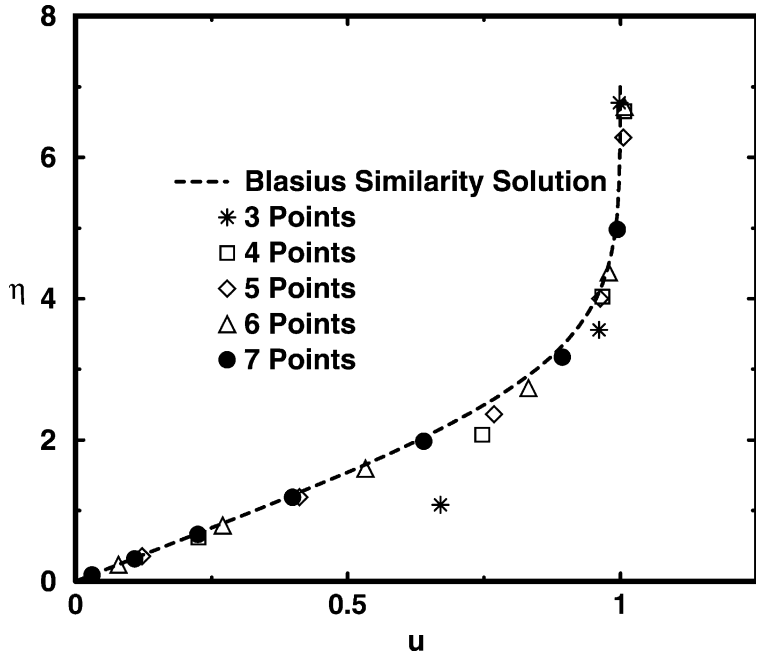

Fig. 5. Effect of normal grid spacing on midchord velocity profile for a flat plate ($M_r = 10^{-3}$).

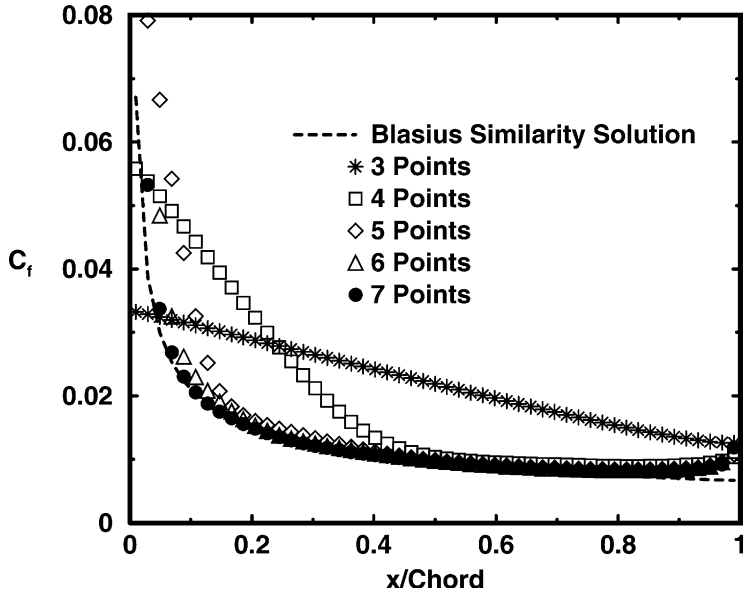

Fig. 6. Effect of normal grid spacing on skin friction coefficient distribution for a flat plate ($M_r = 10^{-3}$).

and fluxes evaluated with algebraic averages. The rectangular grids are (71×21) for laminar flow and (71×41) for turbulent flow, with 50 uniform intervals with spacing $\Delta x = 0.02$ along the unit length of the plate. The normal-direction grid is distributed to provide increased resolution near the wall, with minimum spacing at the wall of $\Delta y = 10^{-4}$ for laminar flow and $\Delta y = 10^{-6}$ for turbulent flow. The grids extend to a distance of 5 lengths upstream and downstream of the leading edge, and 5 lengths to the outer boundary.

In Fig. 7, the convergence behavior is shown for both laminar and turbulent solutions with $M_r = 0.001$, 0.01, 0.1, 0.3. The convergence behavior is essentially independent of Mach number in both cases. The convergence behavior does depend on minimum grid spacing near the wall, however, and this accounts for the difference in convergence rates for laminar and turbulent cases. Multigrid acceleration has significantly improved the convergence rate of a similar flow solver using artificial compressibility [43,44] and is expected improve the present scheme.

In Figs. 8 and 9, the midchord velocity profiles are shown. These are also found to be essentially independent of Mach number and to agree with the Blasius profile for laminar flow and the logarithmic law of the wall for turbulent flow. The influence of different grid spacings normal to the wall is shown in Fig. 10 for the turbulent case. The results in Figs. 5 and 10 demonstrate that the present preconditioned scheme can give reasonably accurate velocity profiles with only five to seven points in the laminar layer and about ten to twenty points in the turbulent layer.

7.3. Flow past a circular cylinder at low Reynolds number

This same flow solver was tested for flow past a circular cylinder for low Reynolds number cases with freestream Mach number $M_\infty M_r = 0.001$. These solutions were computed for an O-grid of size (91×61) with outer boundary located 20 diameters from the cylinder. A time step CFL = 20 was used, with a single Newton iteration and 15 linear subiterations. The convergence behavior for $Re = 1$, 20, and 40 with adiabatic wall, and for $Re = 40$ with $T_w = 5.0$ and 0.2 are shown in Fig. 11, and the converged surface pressure

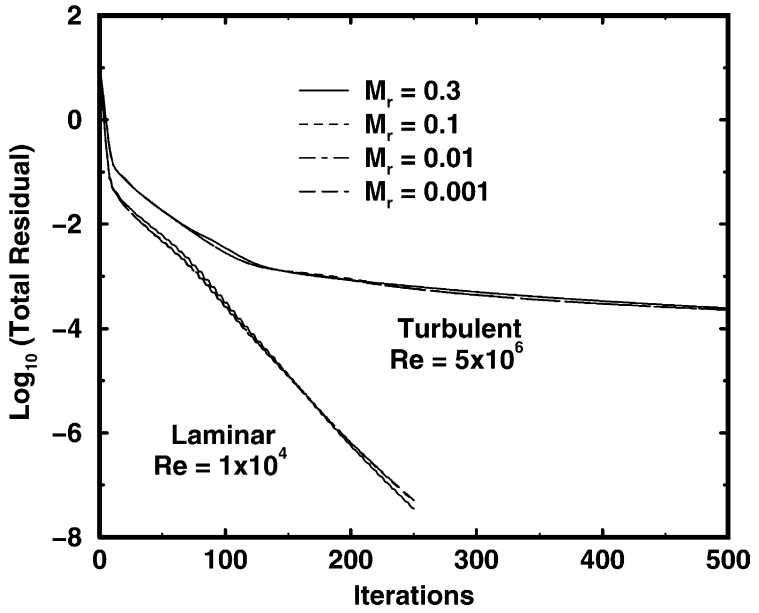

Fig. 7. Convergence behavior for flat-plate boundary layer as influenced by Mach number for the preconditioned scheme ($\beta = M_r^2$).

distributions are compared with experimental measurements of Grove et al. [45] and Fornberg [46] in Fig. 12. Although round-off errors become noticeable for this and smaller Mach numbers, round-off control has not yet been implemented. Choi and Merkle [11] also solved these same adiabatic cases and have given a

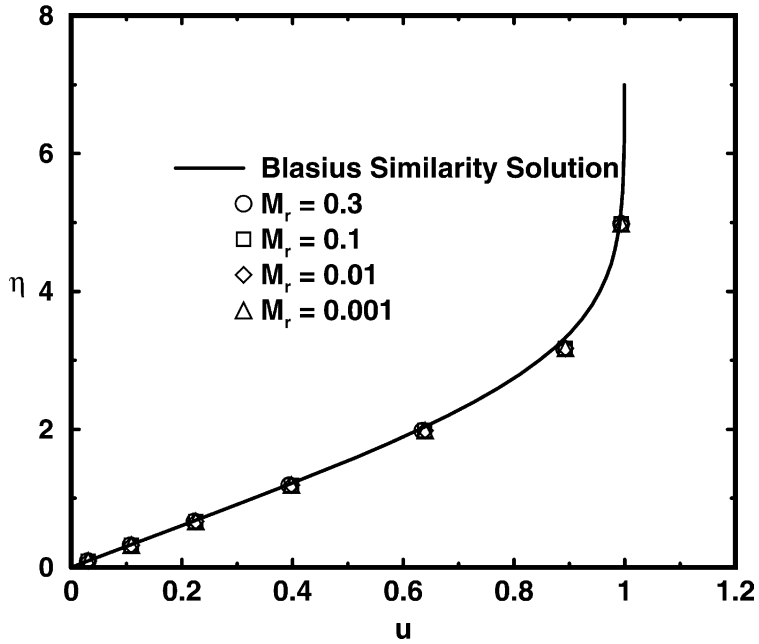

Fig. 8. Midchord laminar velocity profiles as influenced by Mach number ($\beta = M_r^2$).

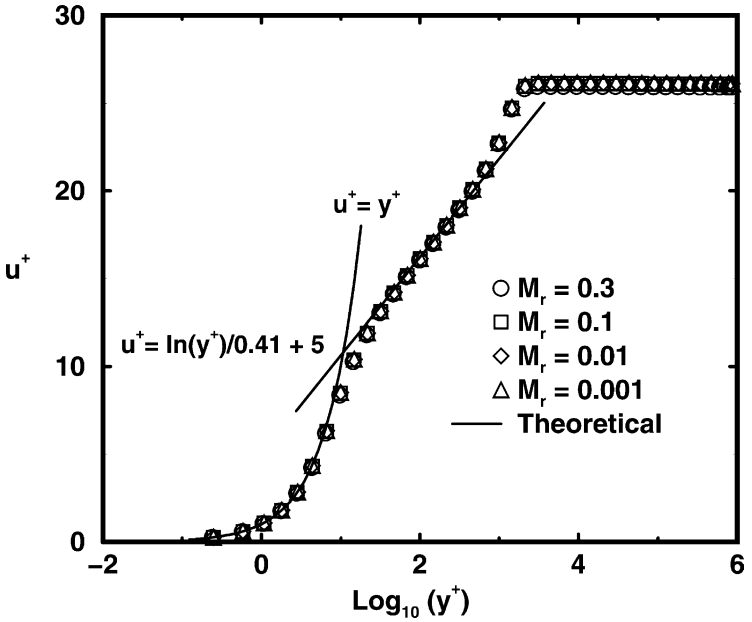

Fig. 9. Midchord turbulent velocity profiles as influenced by Mach number ($\beta = M_r^2$).

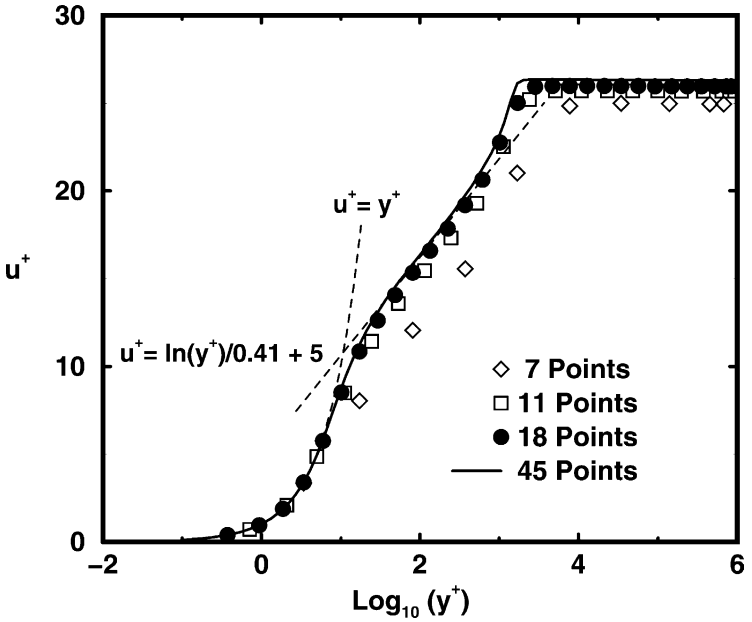

Fig. 10. Effect of normal grid spacing on velocity profile at $x/c = 0.67$ for a flat plate ($M_r = 10^{-3}$).

method to control similar round-off errors. The convergence rates and accuracy observed in Figs. 11 and 12 are reasonable for all flow cases and are comparable to those of [11]. Computed velocity contours for the three adiabatic cases are shown in Fig. 13.

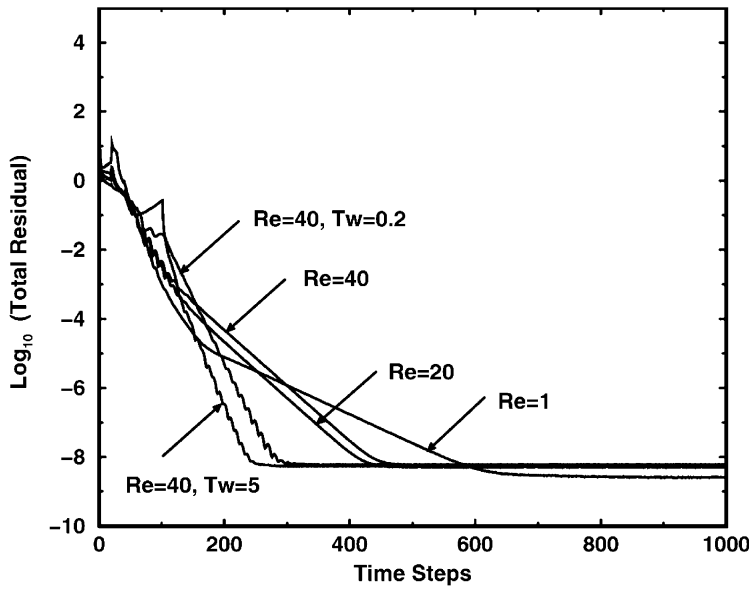

Fig. 11. Convergence behavior for flow past a circular cylinder at ($M_\infty = 10^{-3}$) for $Re = 1$, 20, and 40 with adiabatic wall, and for $Re = 40$ with $T_w = 5.0$ and 0.2 ($M_r = 10^{-3}$, $\beta = M_r^2$).

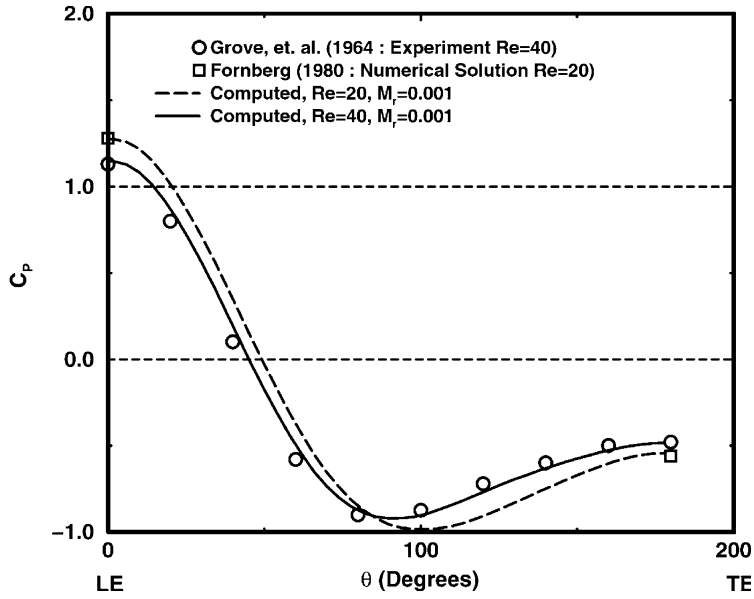

Fig. 12. Flow past a circular cylinder at ($M_\infty = 10^{-3}$): computed surface pressure coefficient, compared with experimental measurements of Grove et al. [45], and Fornberg [46].

8. Validation for transonic and incompressible flows

One motivation for this work has been a single algorithm and code that is applicable to variable Mach number flows ranging from incompressible to supersonic. Accordingly, this section considers the validation

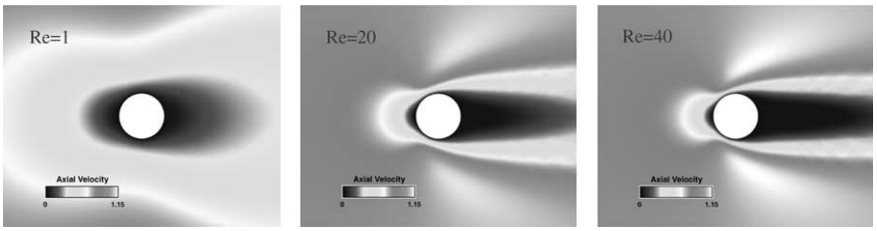

Fig. 13. Flow past a circular cylinder at ($M_\infty = 10^{-3}$): computed velocity contours for $Re = 1$, 20, and 40.

against experimental data for two problems, one an incompressible flow past an axisymmetric submarine hullform known as SUBOFF [47], and the other a transonic flow past a two-dimensional airfoil know as RAE 2822 [48]. These two cases have also been used as validation for an existing compressible flow solver [38], and an incompressible flow solver [44]. These results therefore provide direct validation of the present method by comparison with both experimental data and two completely different computer codes and flow solvers.

8.1. Incompressible flow past an axisymmetric submarine hull

Incompressible (constant density) flows can be closely approximated by using the preconditioned algorithm with a small value of M_r, as shown previously in [3,10] for steady isoenergetic flows. This is possible

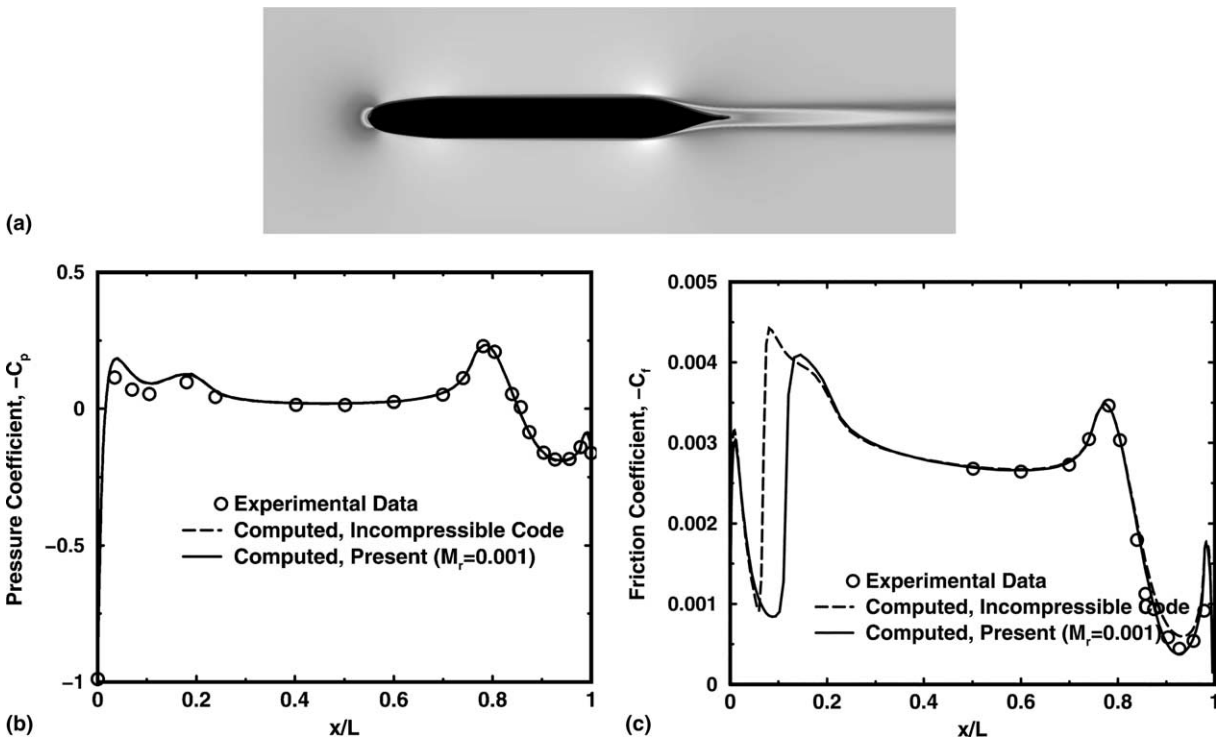

Fig. 14. (a) Flow past the SUBOFF hull at zero incidence: visualization of axial velocity in a vertical cutting plane. (b) Flow past the SUBOFF hull at zero incidence: computed and measured surface pressure coefficient. (c) Flow past the SUBOFF hull at zero incidence: computed and measured friction coefficient.

since the compressible formulation reduces to the incompressible formulation, provided the total enthalpy is constant [3]. The energy equation is included in the present system of equation, and consequently, to approximate an incompressible flow it is only necessary to impose adiabatic boundary conditions and select M_r to be less than about 0.1; the present solution was obtained for $M_r = 0.001$. The SUBOFF hull case has zero incidence and Reynolds number based on hull length of $Re_L = 12 \times 10^6$. The grid size is $(129 \times 65 \times 2)$, with minimum $y^+ < 0.5$, and local time stepping is used with local CFL = 10, 1 Newton iteration, and 5 SGS iterations per time step. Results from this case are shown in Figs. 14(a)–(c).

In Fig. 14(a), computed axial velocity contours are shown for a vertical cutting plane. In Fig. 14(b), the computed surface pressure coefficient is compared both with the experimental data of Huang et al. [47] and with a solution from an existing incompressible code [44]. The agreement is excellent in the area near the stern where viscous effects are important. The difference between the two computed solutions and the data near the bow is attributable to physical entrance effects in the test section of the experiment. In Fig. 14(c), the computed and measured friction coefficients are shown and are generally in good

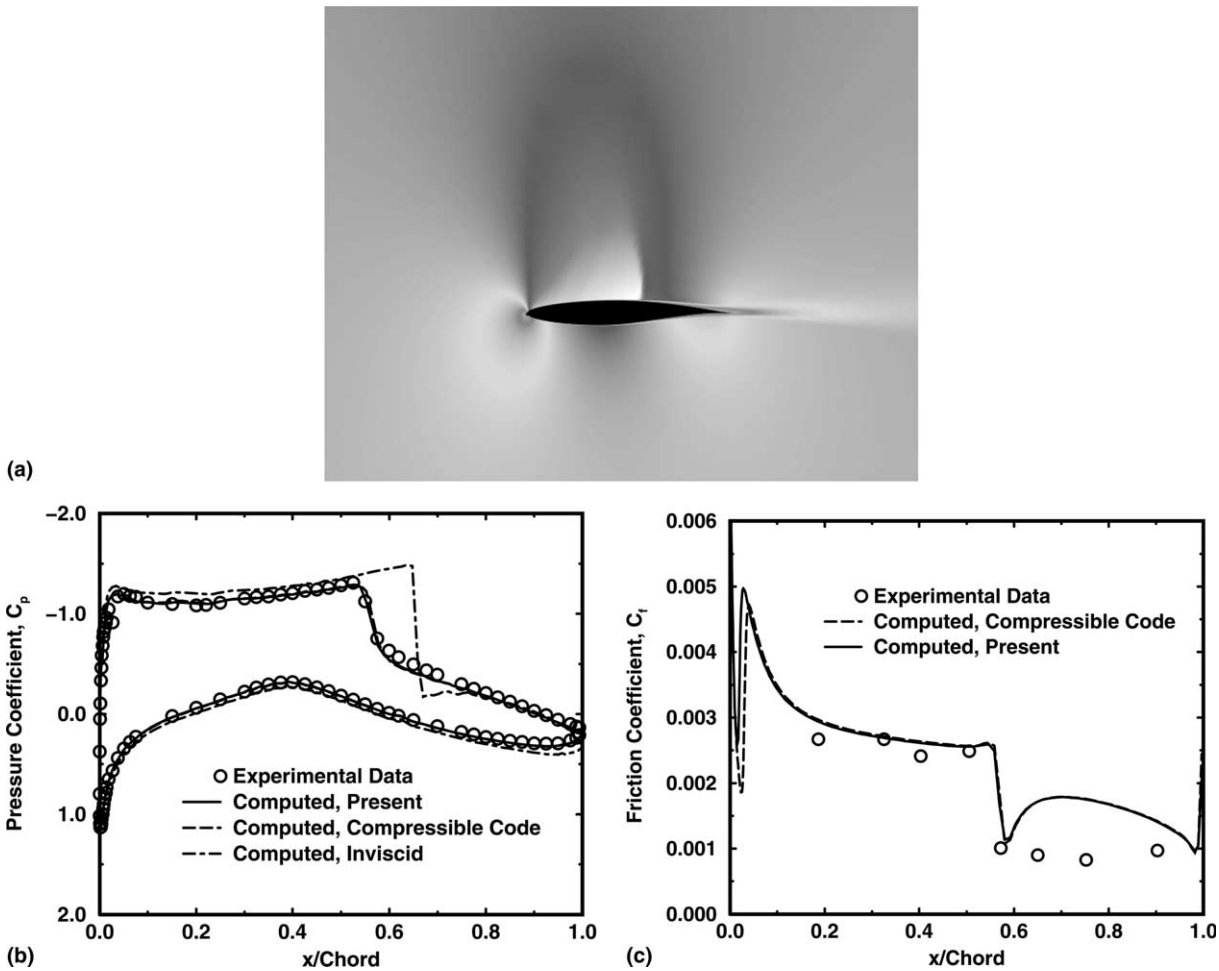

Fig. 15. Flow past an RAE 2822 airfoil at $M_\infty = 0.734°$ and 2.79° incidence ($\beta = M_r^2$): (a) Computed pressure contours. (b) Computed surface pressure coefficient compared with experimental data and solutions for viscous and inviscid flow using an existing compressible code. (c) Computed friction coefficient compared with experimental data and a solution using an existing compressible code.

agreement. The two computed solutions differ near the bow because the turbulent transition point was not forced in these solutions but was allowed to develop according to the turbulence model solution, giving a slightly different transition point for the two solutions. This is not regarded as an accurate prediction of transition.

8.2. Transonic flow past a two-dimensional airfoil

The conditions for the RAE 2822 airfoil are as follows: $M_\infty = M_r = 0.734$, incidence of $\alpha = 2.79°$, and chordal Reynolds number of $Re_c = 6.5 \times 10^6$. The grid size is (481×81), with minimum $y^+ < 1.0$, and local time stepping is used with local CFL = 10, 1 Newton iteration, and 5 SGS iterations, per time step. Results from this case are shown in Figs. 15(a)–(c). Fig. 15(a) shows computed pressure contours. In Fig. 15(b), the computed surface pressure coefficient distribution is compared both with experimental data of Cook et al. [48] and with viscous and inviscid solutions computed with an existing compressible code [38]. The two viscous computations agree well with both the data and with each other, including the location and strength of the shock. The significant differences with the inviscid solution are attributable to strong viscous/inviscid interaction near the shock. In Fig. 15(c), the computed friction coefficients are compared with measurements and agree well except downstream of the shock. The difference in the two computed solutions near the leading edge is again due to a difference in location of the transition point.

9. Concluding remarks

A preconditioned, characteristics-based, primitive-variable, flux-difference formulation has been developed and demonstrated for a range of one and two-dimensional flows. These included an inviscid shock-tube case, flat-plate boundary layer flow at low Mach number, viscous flow past a circular cylinder at low Reynolds number and with different thermal boundary conditions, and validation cases for incompressible and transonic flows. The choices $\boldsymbol{q} = (\rho, u, v, w, p)$ for nondimensional primitive variables, algebraic averages for flux computations, and a simple preconditioning related to a reference Mach number, provide simplicity and preserve slip-line discontinuities. This pre-conditioned viscous flow solver performed well for all problems considered.

Acknowledgements

This work is the culmination of a long-term effort sponsored in part by the National Science Foundation, NASA Ames Research Center, and the Office of Naval Research. This support is greatly appreciated.

Appendix A. Three-dimensional formulation

A.1. Governing equations in general dynamic curvilinear coordinate systems

The unsteady three-dimensional Navier–Stokes equations without body forces are first written in Cartesian coordinates and then transformed to general time-dependent curvilinear coordinates as in

$$\xi = \xi(x, y, z, t), \quad \eta = \eta(x, y, z, t), \quad \zeta = \zeta(x, y, z, t), \quad \tau = t. \tag{A.1}$$

Letting k denote any one of the transformed coordinates ξ, η, ζ, the transformation metrics $\partial k/\partial x$, $\partial k/\partial y$, $\partial k/\partial z$ can be denoted as k_x, k_y, k_z, respectively. It is also convenient to adopt unit grid spacings ($\Delta\xi = \Delta\eta = \Delta\zeta = 1$) for the transformed coordinates. The Navier–Stokes equations can then be written as

$$\boldsymbol{M\Gamma}^{-1}\frac{\partial q}{\partial \tau} + \frac{\partial}{\partial \xi}(\boldsymbol{F} - \boldsymbol{F}_v) + \frac{\partial}{\partial \eta}(\boldsymbol{G} - \boldsymbol{G}_v) + \frac{\partial}{\partial \zeta}(\boldsymbol{H} - \boldsymbol{H}_v) = 0, \tag{A.2}$$

where

$$\boldsymbol{q} = J\begin{bmatrix}\rho\\ u\\ v\\ w\\ p\end{bmatrix}, \quad \boldsymbol{K} = J\begin{bmatrix}\rho\theta_k\\ \rho u\theta_k + k_x p\\ \rho v\theta_k + k_y p\\ \rho w\theta_k + k_z p\\ [e_t + abp]\theta_k - k_t abp\end{bmatrix}, \tag{A.3}$$

$$\boldsymbol{K}_v = J\begin{bmatrix}0\\ T_{kx}\\ T_{ky}\\ T_{kx}\\ Q_k\end{bmatrix},$$

with

$$\begin{aligned}
\theta_k &= k_x u + k_y v + k_z w + k_t,\\
T_{kx} &= k_x\tau_{xx} + k_y\tau_{yx} + k_z\tau_{zx},\\
T_{ky} &= k_x\tau_{xy} + k_y\tau_{yy} + k_z\tau_{zy},\\
T_{kz} &= k_x\tau_{xz} + k_y\tau_{yz} + k_z\tau_{zz},\\
Q_k &= uT_{kx} + vT_{ky} + wT_{kz} + k_x q_x + k_y q_y + k_z q_z
\end{aligned} \tag{A.4}$$

and

$$\begin{aligned}
&K = F, \quad K_v = F_v \quad \text{for } k = \xi,\\
&K = G, \quad K_v = G_v \quad \text{for } k = \eta,\\
&K = H, \quad K_v = H_v \quad \text{for } k = \zeta.
\end{aligned} \tag{A.5}$$

Here, $a \equiv \gamma - 1$ and $b \equiv M_r^2$ are constants, and τ_{kx}, τ_{ky}, τ_{kz}, and q_k denote thin-layer approximations for shearing stress and heat flux. The Jacobian of the inverse transformation $\partial(x, y, z, t)/\partial(\xi, \eta, \zeta, \tau)$ is given by

$$J = x_\xi(y_\eta z_\zeta - z_\eta y_\zeta) - y_\xi(x_\eta z_\zeta - z_\eta x_\zeta) + z_\xi(x_\eta y_\zeta - y_\eta x_\zeta). \tag{A.6}$$

A.2. Preconditioned matrices and eigensystems for $\boldsymbol{q} = (\rho, u, v, w, p)$ variables

The preconditioning matrix is given by

$$\boldsymbol{\Gamma} = \mathrm{diag}(1, 1, 1, 1, \beta). \tag{A.7}$$

The Jacobian for the change to primitive variables is

$$\boldsymbol{M} = \begin{bmatrix} 1 & 0 & 0 & 0 & 0 \\ u & \rho & 0 & 0 & 0 \\ v & 0 & \rho & 0 & 0 \\ w & 0 & 0 & \rho & 0 \\ ab\phi & ab\rho u & ab\rho v & ab\rho w & b \end{bmatrix}, \tag{A.8}$$

where $\phi \equiv (u^2 + v^2 + w^2)/2$. The system matrix is

$$\boldsymbol{\Gamma a} = \begin{bmatrix} \theta_k & \rho k_x & \rho k_y & \rho k_z & 0 \\ 0 & \theta_k & 0 & 0 & k_x/\rho \\ 0 & 0 & \theta_k & 0 & k_y/\rho \\ 0 & 0 & 0 & \theta_k & k_z/\rho \\ 0 & \beta k_x \rho c^2 & \beta k_y \rho c^2 & \beta k_z \rho c^2 & \beta\theta_k \end{bmatrix}. \tag{A.9}$$

The eigenvalues $\boldsymbol{\Gamma a}$ are

$$\lambda_k = \theta_k, \theta_k, \theta_k, \theta_k\beta^+ + \sigma, \theta_k\beta^+ - \sigma, \tag{A.10}$$

where

$$\sigma^2 \equiv (\theta_k\beta^-)^2 + \beta c^2 \tag{A.11}$$

with $\beta^\pm \equiv (1 \pm \beta)/2$. A nonsingular set of right eigenvectors for $\boldsymbol{\Gamma a}$ is given by

$$\boldsymbol{R}_k = \begin{bmatrix} k_x & k_y & k_z & \frac{\rho}{\beta c^2}(\theta_k\beta^- + \sigma) & \frac{-\rho}{\beta c^2}(\theta_k\beta^- - \sigma) \\ 0 & -k_z & k_y & k_x & -k_x \\ k_z & 0 & -k_x & k_y & -k_y \\ -k_y & k_x & 0 & k_z & -k_z \\ 0 & 0 & 0 & -\rho(\theta_k\beta^- - \sigma) & \rho(\theta_k\beta^- + \sigma) \end{bmatrix}. \tag{A.12}$$

References

[1] E. Turkel, A review of preconditioning methods for fluid dynamics, Appl. Numer. Math. 12 (1993) 257–284.
[2] E. Turkel, Preconditioning techniques in computational fluid dynamics, Annu. Rev. Fluid Mech. 31 (1999) 385–416.
[3] W.R. Briley, H. McDonald, S.J. Shamroth, A low Mach number Euler formulation and application to time iterative LBI schemes, AIAA J. 21 (10) (1983) 1467–1469.
[4] H. McDonald, W.R. Briley, Three-dimensional supersonic flow of a viscous or inviscid gas, J. Comp. Phys. 19 (2) (1975) 150–178.
[5] J.L. Steger, P. Kutler, Implicit finite-difference procedures for the computation of vortex wakes, AIAA J. 15 (4) (1977) 581–590.
[6] D. Choi, C.L. Merkle, Application of time-iterative schemes to incompressible flow, AIAA J. 23 (10) (1985) 1518–1524.
[7] C.L. Merkle, D.L. Choi, Computation of low-speed flow with heat addition, AIAA J. 25 (6) (1987) 831–838.
[8] H. Viviand, Pseudo-unsteady systems for steady inviscid flow calculation, in: F. Angrand, et al. (Eds.), Numerical Methods for the Euler Equations of Fluid Dynamics, SIAM, Philadelphia, 1985.
[9] E. Turkel, Preconditioned methods for solving the incompressible and low-speed compressible equations, J. Comput. Phys. 72 (1987) 277–298.
[10] W.R. Briley, R.C. Buggeln, H. McDonald, Solution of the incompressible Navier–Stokes equations using artificial compressibility, in: Proceedings of the Eleventh International Conference on Numerical Methods in Fluid Mechanics, Springer, New York, 1989.
[11] Y.H. Choi, C.L. Merkle, The application of preconditioning to viscous flows, J. Comput. Phys. 105 (1993) 207–223.
[12] J.M. Weiss, W.A. Smith, Preconditioning applied to variable and constant density flows, AIAA J. 33 (1995) 2050–2057.
[13] J.M. Weiss, J.P. Maruszewski, W.A. Smith, Implicit solution of preconditioned Navier–Stokes equations using algebraic multigrid, AIAA J. 37 (1999) 29–36.

[14] R.H. Pletcher, K.-H. Chen, On solving the compressible Navier–Stokes equations for unsteady flows at very low Mach number, AIAA Paper No. 93-3368-CP, 1993.
[15] J.R. Edwards, M-S. Liou, Low-diffusion flux-splitting methods for flows at all speeds, AIAA J. 36 (9) (1998) 1610–1617.
[16] J.R. Edwards, J.L. Thomas, Development and investigation of $O(Nm^2)$ preconditioned multigrid solvers for the Euler and Navier–Stokes equations, AIAA Paper No. 99-3263, 1999.
[17] P.L. Roe, Characteristic-based schemes for the Euler equations, Ann. Rev. Fluid Mech. 18 (1986) 337–365, Annual Reviews.
[18] E.F. Toro, Riemann Solvers and Numerical Methods for Fluid Dynamics, second ed., Springer, Berlin, 1999.
[19] P.L. Roe, Approximate Riemann solvers, parameter vector, and difference schemes, J. Comput. Phys. 43 (1981) 357.
[20] M.-S. Liou, C.J. Steffan, A new flux splitting scheme, J. Comput. Phys. 107 (1993) 23.
[21] L.B. Simpson, D.L. Whitfield, Flux-difference split algorithm for unsteady thin-layer Navier–Stokes solutions, AIAA J. 30 (4) (1992) 914–922.
[22] D.L. Whitfield, L.K. Taylor, Discretized Newton-relaxation solution of high-resolution flux-difference split schemes, AIAA Paper No. 91–1539, 1991.
[23] L.K. Taylor, D.L. Whitfield, Unsteady three-dimensional incompressible Euler and Navier–Stokes solver for stationary and dynamic grids, AIAA Paper No. 91–1650, 1991.
[24] D.L. Whitfield, L.K. Taylor, Numerical solution of the two-dimensional time-dependent incompressible Euler equations, Mississippi State University Report No. MSSU-EIRS-ERC-93-14, 1994.
[25] S.R. Chakravarthy, Relaxation methods for unfactored implicit upwind schemes, AIAA Paper 84–0165, 1984.
[26] M.M. Rai, A relaxation approach to patched grid calculations with the Euler equations, J. Comp. Phys. 66 (1986) 99–131.
[27] D. Pan, S. Chakravarthy, Unified formulation for incompressible flows, AIAA Paper 89-0122, 1989.
[28] S.E. Rogers, D. Kwak, An upwind differencing scheme for the time-accurate incompressible Navier–Stokes equations, AIAA J. 28 (2) (1990) 253–262.
[29] L.K. Taylor, J.A. Busby, M.Y. Jiang, A. Arabshahi, K. Sreenivas, D.L. Whitfield, Time accurate incompressible Navier–Stokes simulation of the flapping foil experiment, in: Proceedings of the Sixth International Conference on Numerical Ship Hydrodynamics, Iowa City, IA, 1993.
[30] R. Pankajakshan, L.K. Taylor, C. Sheng, W.R. Briley, D.L. Whitfield, Scalable parallel implicit multigrid solution of unsteady incompressible flows, in: D.A. Caughey, M.M. Hafez (Eds.), Frontiers of Computational Fluid Dynamics 2002, World Scientific, PTE LTD, Singapore, 2002.
[31] A. Jameson, E. Turkel, Implicit schemes and LU decompositions, Math. Comp. 37 (1981) 385.
[32] E.K. Buratynski, D.A. Caughey, An implicit LU scheme for the Euler equations applied to arbitrary cascades, AIAA Paper 84-0167, 1984.
[33] A. Jameson, S. Yoon, Lower–upper implicit schemes with multiple grids for the Euler equations, AIAA J. 25 (7) (1987) 929–935.
[34] S. Yoon, A. Jameson, Lower–upper symmetric Gauss–Seidel method for the Euler and Navier–Stokes equations, AIAA J. 26 (9) (1988) 1025–1026.
[35] S. Yoon, D. Kwak, Three-dimensional incompressible Navier–Stokes solver using lower–upper symmetric Gauss–Seidel algorithm, AIAA J. 29 (6) (1991) 874–875.
[36] W.R. Briley, H. McDonald, An overview and generalization of implicit Navier–Stokes algorithms and approximate factorization, Comput. Fluids 30 (2001) 807–828.
[37] W.K. Anderson, J.T. Thomas, B. van Leer, Comparison of finite volume flux vector splittings for the Euler equations, AIAA J. 24 (1986) 1453.
[38] A. Arabshahi, J.M. Janus, A multiblock compressible Navier–Stokes flow solver applied to complex launch vehicles, AIAA-99-3378, 1999.
[39] J.J. Quirk, A contribution to the great Riemann solver debate, NASA CR 191409, ICASE Report No. 92–64, 1992.
[40] M.-S. Liou, Mass flux schemes and connection to shock instability, J. Comp. Phys. 160 (2000) 623–648.
[41] T.J. Coakley, Turbulence modeling methods for the compressible Navier–Stokes equations, AIAA Paper No. 83–1693, 1983.
[42] T.J. Coakley, T. Hsieh, A comparison between implicit and hybrid methods for the calculation of steady and unsteady inlet flows, AIAA Paper No. 85–1125, 1985.
[43] C. Sheng, L.K. Taylor, D.L. Whitfield, An efficient multigrid acceleration for solving the 3-D incompressible Navier–Stokes equations in generalized curvilinear coordinates, AIAA Paper No. 94–2335, 1994.
[44] R. Pankajakshan, L.K. Taylor, C. Sheng, M.J. Jiang, W.R. Briley, D.L. Whitfield, Parallel efficiency in implicit multiblock, multigrid simulations, with application to submarine maneuvering, AIAA Paper 2001-1093, 2001.
[45] A.S. Grove, F.H. Shair, E.E. Peterson, A. Acrivos, J. Fluid Mech. 19 (1964) 60.
[46] B. Fornberg, J. Fluid Mech. 98 (1980) 819.
[47] T.T. Huang, H.-L. Liu, N.C. Groves, T.J. Forlini, J.N. Blanton, S. Gowing, Measurement of flows over an axisymmetric body with various appendages, in: Nineteenth Symposium on Naval Hydrodynamics, Seoul, Korea, 1992.
[48] P.J. Cook, M.A. McDonald, M.C.P. Firmin, Aerofoil RAE 2822 – Pressure distributions and boundary layer and wake measurements, AGARD-AR-138, 1979.